

AMERICAN UNIVERSITY OF BEIRUT

EFFICIENT RF WAKE-UP AND CHARGING
OF IOT DEVICES USING AMBIENT WI-FI
SIGNALS

by

SANDY HASSAN SAAB

A thesis

submitted in partial fulfillment of the requirements
for the degree of Master of Engineering
to the Department of Electrical and Computer Engineering
of the Faculty of Engineering and Architecture
at the American University of Beirut

Beirut, Lebanon
May 2018

AMERICAN UNIVERSITY OF BEIRUT

EFFICIENT RF WAKE-UP AND CHARGING
OF IOT DEVICES USING AMBIENT WI-FI
SIGNALS

by
SANDY HASSAN SAAB


Approved by:

Prof. Zaher Dawy, Professor
Electrical and Computer Engineering




Advisor

Prof. Joseph Costantine, Associate Professor
Electrical and Computer Engineering




co-Advisor

Prof. Rabih Jabr, Professor
Electrical and Computer Engineering



Member of Committee

Prof. Imad El Hajj, Professor
Electrical and Computer Engineering



Member of Committee

Date of thesis defense: May 3, 2018

Acknowledgements

First, I would like to thank God for being with me every step of the way. He always guided me and gave me the strength to dream big and achieve my goals and ambitions.

I would like to express my recognition and sincere gratitude to my advisors Prof. Zaher Dawy and Prof. Joseph Costantine for their continuous support, motivation, and supervision during the last two years. Their professionalism is the key element in the success of this work.

Also, I would like to address full appreciation to the rest of my thesis committee: Prof. Rabih Jabr, and Prof. Imad El Hajj for their dedication and encouragement.

I would like to thank the members of the wireless communication and Radio Frequency Lab at the American University of Beirut for their continuous support and efforts exerted in the preparation of the testing area. Also, I would like to express my gratitude to Ms. Aline Eid and Dr. Nour Kouzayha for all their help, encouragement, continuous dedication, and for the extensive research-related discussions that we held.

Last but not least, my deepest gratitude goes to my family members who were patient enough to supply me continuously with unlimited love and confidence.

An Abstract of the Thesis of

Sandy Hassan Saab for Master of Engineering
Major: Electrical and Computer Engineering

Title: Efficient RF Wake-Up and Charging of IoT Devices Using Ambient Wi-Fi Signals

The internet of things (IoT) is based on the deployment of a wide range of sensor devices in various use cases that include smart cities, autonomous cars, mobile health, and agricultural and environmental monitoring. Sensor devices are usually battery operated and can be located in hard-to-reach areas, which limits the ability to charge or replace their batteries. The main aim of this thesis is to design, implement and evaluate an effective solution for harvesting energy from Wi-Fi routers by converting ambient RF signals into DC output that can be used to wake up the sensor device from a deep sleep mode or to charge its battery.

The proposed solution includes two main components: (i) a rectifier circuit to harvest RF energy, with design options based on both passive and active components; (ii) an algorithm to control the data transmission from the Wi-Fi router in order to generate a signal profile that is suitable for achieving high efficiency in the rectifier circuit. Extensive experimental testing is performed in order to analyze the performance trade-offs as a function of various system parameters including the separation distance between the Wi-Fi router and the sensor device. In addition, we optimize the performance of the proposed algorithm to minimize the effect on other users streaming content from the same Wi-Fi router. We also perform experiments to demonstrate the positive effect of interference from multiple Wi-Fi routers located in the vicinity of the sensor device. Finally, we present a case study on smart farming to demonstrate the functionality and effectiveness of our designed solution in waking up and recharging a sensor that is deployed in a field, including experiments to quantify the impact of losses due to deploying the sensor under ground level at various depths.

Contents

Acknowledgements	v
Abstract	vi
1 Introduction	1
2 Literature Review	5
2.1 Wake-Up Radio	5
2.2 Wake-Up Receivers and RF Energy Harvesting	6
3 RF Energy Harvesting from Ambient Wi-Fi Signals	10
3.1 System Model and Definitions	10
3.2 Challenges of Harvesting Wi-Fi Signals	10
3.3 Software Based Router Data Transmission	13
3.3.1 Ambient Vs. Dedicated Transmission	13
3.3.2 Efficiency Response With Respect To Wi-Fi Channels	16
3.3.3 Efficiency Response With Respect To Distance	16
3.4 Effect on Active Wi-Fi Users	17
3.4.1 System Overview and Parameter Definitions	17
3.4.2 Efficiency and Network Performance	19
4 Positive Effect of Interference	25
4.1 Experimental Setup	26
4.1.1 Setup 1: Three APs at Various Distances	29
4.1.2 Setup 2: Three APs Next to Each Other	30
4.1.3 Setup 3: Three APs Behind Each Other	31
4.1.4 Comparative Analysis Between Setups	32
5 Power Management Circuit	33
5.1 Existing RF Based Wake-Up Circuit With Active Components	33
5.2 RF Wake-Up Circuit Design Enhancements Using Active Components	35
5.2.1 Ultra-Low Input Current Amplifier Characteristics	35

5.3	RF Wake-Up Circuit Comparison Between Existing and Enhanced Designs	41
5.4	RF Charging Circuit Design Using Passive Components	42
5.4.1	DC-DC Power Converter Characteristics	42
5.4.2	Performance of Designed Passive System	44
5.4.3	Charging a Battery from a Passive Circuit	47
5.5	Comparative Study Between Active and Passive Setups	48
6	Case Study: Smart Agriculture	50
6.1	Indoor Experiment in Lossless Media	50
6.2	Outdoor Experiment in Lossy Underground Media	51
6.3	Experimental Setup	52
6.3.1	Fine Sand and WUSN	53
6.4	Remote Sensing Using A Drone	56
6.4.1	Drone's Flying Approach 1: Vertical	57
6.4.2	Drone's Flying Approach 2: Raster	59
6.4.3	Comparison Between Approach 1 and 2	60
7	Conclusion and Future Work	61
A	Abbreviations	63

List of Figures

1.1	System model.	2
1.2	RF energy harvesting circuit.	3
2.1	Complete node with Wake-up Radio.	6
3.1	Block diagram of an RF wake-up device.	11
3.2	Block diagrams of an RF powered device.	11
3.3	Router's normal activity.	12
3.4	Router's packet rate with and without packet injection.	14
3.5	Ambient harvesting setup.	14
3.6	Dedicated harvesting setup.	15
3.7	Efficiency comparison between dedicated and ambient scenarios.	15
3.8	Efficiency results for the rectifier with proposed matching technique.	15
3.9	Measured PCE results with respect to frequency for different received power levels.	16
3.10	Measured PCE and received power results with respect to distance.	17
3.11	Samsung S4 devices streaming data from the Wi-Fi access point.	18
3.12	Number of packets sent over a period of 10sec while varying the packet size and interpacket delay.	19
3.13	Number of packets sent and efficiency for a packet size of 700B over different inter-packet delay duration.	20
3.14	Number of packets sent and efficiency for a packet size of 1000B over different inter-packet delay duration.	20
3.15	Number of packets sent and efficiency for a packet size of 1500B over different inter-packet delay duration.	21
3.16	Packet Success Ratio.	22
3.17	Packet Received Ratio.	22
3.18	Download duration and DC voltage as function of the packet size.	23
3.19	Download bit rate and DC voltage as function of the packet size.	23
3.20	Download bit rate and DC voltage as function of the inter-packet delay.	24
3.21	Download duration and DC voltage as function of the inter-packet delay.	24

4.1	System model.	25
4.2	Effect of interference setup.	26
4.3	2x1 meandered line antenna array.	27
4.4	Meandered line antenna's radiation pattern.	27
4.5	Omnidirectional antenna.	28
4.6	Omnidirectional antenna's radiation pattern.	28
4.7	Experimental setup 1: Monitoring the Pr level from 3 APs placed at different distances from one another.	29
4.8	Results of setup 1: Pr on meander vs. omnidirectional antenna from 3 APs at different distances.	29
4.9	Experimental setup 2: Monitoring the Pr level from 3 APs placed next to each other.	30
4.10	Results of setup 2: Pr on meander vs. omnidirectional antenna from 3 APs placed next to each other.	30
4.11	Experimental Setup 3: Monitoring the Pr level from 3 APs placed behind each other.	31
4.12	Results of setup 3: Pr on meander vs. omnidirectional antenna from 3 APs behind each other.	31
4.13	Comparing the Pr level when using 1 AP and 3 APs.	32
5.1	LTC1540 circuit diagram.	33
5.2	Prototype of the wake-up receiver [50].	34
5.3	LMC6001 circuit diagram.	36
5.4	The LMC6001 in its comparator mode at 2mV threshold voltage simulated on Proteus.	37
5.5	The LMC6001 in its comparator mode at 100mV threshold voltage simulated on Proteus.	37
5.6	In lab measured distance for the designed wake-up circuit.	38
5.7	Measured distance and output voltage of the wake-up circuit design.	38
5.8	Current consumed by the active wake-up circuit.	39
5.9	Measured power received level of the wake-up circuit design by the signal generator.	39
5.10	Rectenna and the LMC6001 anechoic chamber testing.	40
5.11	LTC3108 input current and voltage behavior for different transformer windings [53].	43
5.12	DC-DC boost composed of a 1:20 transformer, C1=10nF, C2=330pF, C3=1μF, and C4=10μF.	44
5.13	Fabricated DC-DC boost.	45
5.14	Testing the functionality of the fabricated DC-DC boost.	45
5.15	Maximum charging distance using the passive system.	46
5.16	Charging duration of a 300mAh NiCd battery.	47
5.17	Comparing the charging and wake-up capabilities for increasing energy efficiency and distance.	49

6.1	DC voltage as function of the wake-up distance of the indoor experiment.	51
6.2	Experimental setup of sensors buried in dry sand and slightly wet sand.	53
6.3	Rectenna packaging.	54
6.4	Distance from the router to the pipe.	54
6.5	voltage is measured as the rectenna is lowered in the pipe and covered with sand.	55
6.6	Comparing the voltage results of the rectenna when buried either under dry sand or under slightly wet sand.	55
6.7	RF energy harvesting from the drone's telemetry signals.	56
6.8	Sensor system composed of a rectifier and a 3dB patch antenna.	57
6.9	Vertical approach: Drone flying over the field starting at an altitude of 15m and reaching 5m.	58
6.10	Vertical approach: Voltage received.	58
6.11	Vertical approach: Wake-Up distance.	59
6.12	Raster approach: Voltage received.	59
6.13	Vertical and Raster approach distance variations and maximum achieved voltage.	60

List of Tables

- 5.1 Measured current(μA) and power(μW) consumption for design 1. 41
- 5.2 Evaluating the life time of design [50] and design 1 with respect to the wake-up receiver and microcontroller's current only. 41
- 5.3 Evaluating [50] and this work with respect to different parameters. 42
- 5.4 VS1 and VS2 different configurations that can change the voltage at the output of the DC-DC boost. 43
- 5.5 Different Tx power, and antenna gains. 46

Chapter 1

Introduction

With the recent advancements in wireless communications, it is expected that 50 billion devices will be connected worldwide by 2020 [1]. The Internet of Things (IoT) is the key to this evolution since it allows both Machine to Machine(M2M) and Machine to Person (M2P) connectivity [1]. Mainly, IoT is defined as a smart network with a large number of inter-connected things or objects, such as sensors, mobile handsets, actuators, etc. These smart devices provide intelligent everyday services such as e-health, automated control, energy management (smart city and smart grid), logistics, security control, safety management and smart agriculture.

In wireless environments, transmission and reception costs could drain system power and this problem motivates research efforts to find practical and efficient solutions to reduce power consumption. Mainly, Wireless Sensor Networks (WSN) are powered by batteries and this restricts the sensors' performance because of the batteries limited energy storage capability. Although battery replacement provides an intermediate solution to energy shortage, frequent replacement of batteries can be costly and cumbersome which creates a serious performance bottleneck in providing stable communication services. Therefore, extending the lifetime of IoT devices becomes crucial for the recognition of the IoT vision [2].

A promising approach to extend the lifetime of wireless communication networks is to equip IoT devices with wireless energy harvesting (WEH) technology to scavenge energy from external sources. Solar, wind, tidal, biomass, photovoltaic, kinetic and geothermal are the major renewable energy sources for harvesting [3, 4]. Yet, these conventional natural energy sources are usually climate and location dependent which limits the mobility of the IoT devices. Among the WEH techniques, RF energy harvesting has recently emerged as a practical and effective solution to maintain energy efficiency and perpetual communication in self-sustainable IoT networks[5, 6]. With this technology, IoT devices are enabled to scavenge energy from RF signals broadcasted by ambient sources to support their operation.

The work in this thesis focuses on expanding the potential of RF energy harvesting to efficiently wake-up and charge IoT devices. The goal of this work

is to collect ambient Wi-Fi signals and convert them into DC power and supply small electrical and portable devices with charging capabilities. Hence, RF energy harvesting results in creating self-sustainable wireless devices.

Fig. 1.1 shows the adopted system model of ambient RF energy harvesting where commercial Wi-Fi routers are used to deliver energy to IoT devices. In the proposed system, the IoT device is equipped with a Wake-up Radio (WuR) circuit that can harvest energy from RF signals and use this energy to activate the device. In order to improve the energy efficiency of the device, the power consumption of this circuit is designed to be extremely low. An IoT device that employs the wake-up concept is called an RF wake-up device and an IoT device that employs the charging concept is an RF powered device.

In an RF energy harvesting system, the rectenna which is a combination of the rectifier and the antenna is the most important element. Fig. 1.2 presents an RF energy harvesting circuit that is composed of an antenna, a rectifier that converts RF power into DC voltage, and a power management circuit. The antenna is the front end of the receiver and it captures the signals and feeds them to an efficient rectifying circuit. The harvested energy is then rectified and converted to DC power. The recovered DC power, either wakes up a low powered device directly, or charges a capacitor or a battery. The adopted technique is the key behind

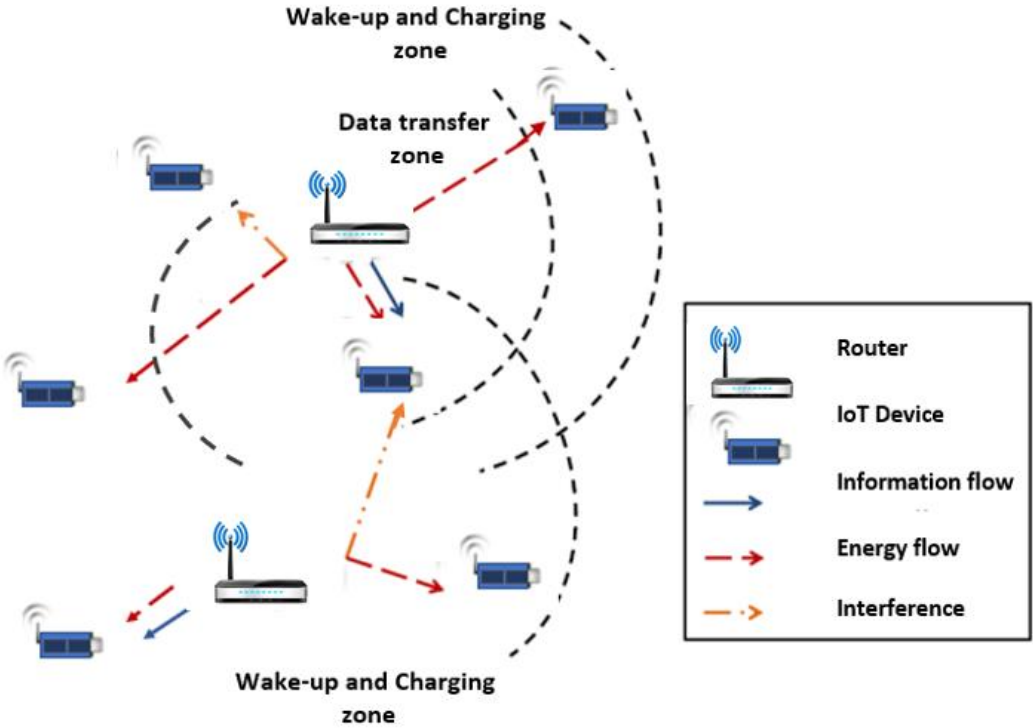


Figure 1.1: System model.

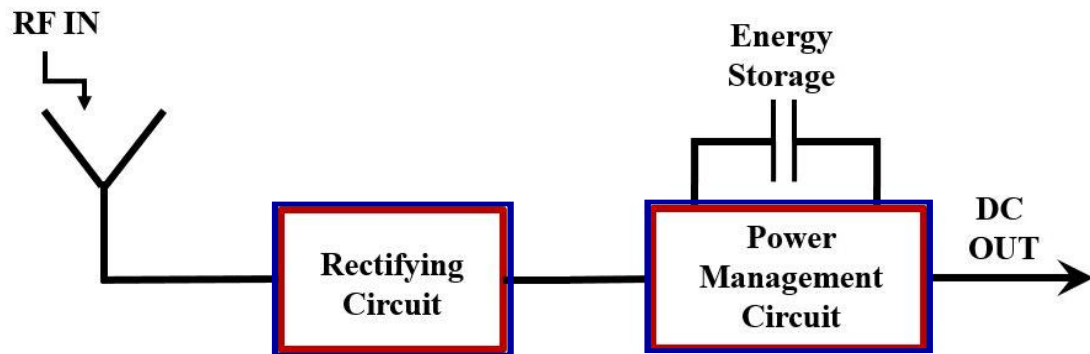


Figure 1.2: RF energy harvesting circuit.

wireless charging or wireless power transfer from RF energy. It also constitutes a great advantage for any distant or mobile devices.

Furthermore, Wi-Fi transmissions are based on the alternation between continuous and silent transmission periods. This is a main impediment that limits the rectenna circuit's performance since the antenna would not capture a continuous and steady signal.

Therefore, the work in this thesis focuses on the design, implementation and optimization of a novel software based approach that allows Wi-Fi signals from any commercial access points (AP) to power IoT devices. This new approach eliminates the silent periods' restrictions by increasing the channel occupancy to achieve continuous transmission that leads to efficient rectification. Therefore, it provides a novel and effective tool for wireless charging from ambient Wi-Fi signals.

The work in this thesis also introduces two different power management units. Each design is integrated with the rectenna system and is optimized for a given set of parameters. Comparative analysis under realistic case studies highlights the enhancements and the different use cases of each designed circuit. This work is then extended to an agriculture use case where extensive collected measurements demonstrate the effectiveness and practicality of our system in facilitating efficient wake-up in underground wireless sensor networks. Moreover, for the case of remote sensing, a drone is used to successfully wake-up sensor devices.

This thesis is composed of seven chapters that are divided as follows: Chapter II carries out a survey on wake-up radio and RF energy harvesting systems. It serves as a general description of the techniques that are presented in the literature. Chapter III introduces ambient RF energy harvesting along with its challenges. It also presents a novel software defined algorithm that will enable energy harvesting of Wi-Fi signals. Chapter IV highlights the positive effect of interference on RF energy harvesting. Chapter V discusses the trade-offs between the different designed power management units. In Chapter VI, indoor experi-

ments are conducted to verify the capability of waking up environmental sensors in lossless media. Also, in this chapter a case study that focuses on the ability to wake-up wireless underground sensor networks is introduced. Finally, Chapter VII ends with a conclusion that summarizes the main results of the thesis and highlights future research directions.

Chapter 2

Literature Review

The objective of this literature survey is to give a general overview about some important concepts related to the thesis work. It serves as a general description of the system models and techniques that are presented in the literature.

We start by giving a general overview about WuR. Then a detailed description related to work done on wake-up receivers (WuRx) and RF energy harvesting.

2.1 Wake-Up Radio

Traditionally, the introduction of low-power radios and duty-cycling Medium Access Protocols (MAC) served as an initial solution for the power limitation issue [2]. In duty-cycling, the nodes are woken up periodically only to transmit or receive data. However, the duty-cycling MAC cant extend the lifetime of a sensor node because the consumption of low-power wireless radios is more or less the same when listening for transmissions and when transmitting. For example, the CC2420 radio model can consume 21.8mA in listening mode and 19.5mA in transmission mode [7]. Consequently, if this radio is always on either listening or transmitting, its power will deplete in almost a week. During the sleep intervals, data latency becomes a serious problem because new information can only be transmitted when the node is awake. Duty-cycling also introduces time synchronization overhead to ensure that transmitters send only when the node receivers wake up. According to [7], researchers have developed many new MAC protocols to solve the problems accompanying duty-cycling. However, these protocols remain unsuitable for delay sensitive and event driven applications as well as extending the lifetime duration of a sensor node.

Consequently, idle-listening was proposed wherein the main receiver is switched off. The main radio transceiver is connected to a WuRx that can detect a possible incoming transmission. Once a wake-up signal (WuS) or an interrupt is received by the WuRx, the main radio switches on and conducts the necessary computations [2]. Fig. 2.1 presents a WuR transceiver integrated with a traditional

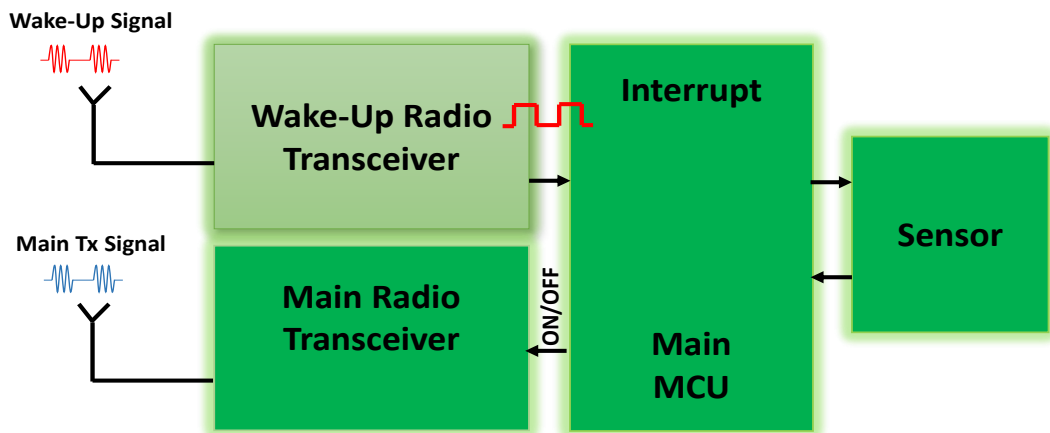


Figure 2.1: Complete node with Wake-up Radio.

sensor node consisting of the main radio transceiver, a microcontroller and a sensor. The WuR is considered a promising solution and it is increasingly deployed as part of WSN. WuRs are expected to illuminate the problems of latency and asynchronous transmission.

Since WuRs consume few micro watts, they are always on while the sensor is always sleeping. Thus, WuR reduces energy wastage since the main radio is on when there is a need to transmit only. Furthermore, in order for a WuR to function efficiently in a multi-user environment, it should wake-up with minimum latency especially in applications evolving health-care. WuRx must maintain low power consumption, even in active mode, as well as a good balance between power used and power saved [8].

Of course, false wake-up and interference will result in significant energy waste, so addressing methods and decoding techniques are conducted to trigger only the intended nodes when a WuS is received. Furthermore, an enhanced processing capability will help filter out the noise and interference to avoid erroneous wake-up.

2.2 Wake-Up Receivers and RF Energy Harvesting

According to [9], energy efficiency is significantly improved by recycling the ambient RF signals that are broadcasted from different sources such as base stations, radio/television stations, hand-held radio, access points and mobile phones. Basically, extracting energy from available RF signals maintains permanent conservation and battery-free implementation of IoT devices. Moreover, since the wireless energy is transferred with the same RF signals that deliver information, energy

harvesting becomes an appropriate possible solution that can power IoT devices [10, 11, 12, 13]. Recently, simultaneous wireless information and power transfer (SWIPT) has drawn considerable attention among researchers and has been strongly investigated [14]. The emerging self-sustainable communications with RF energy harvesting has found its applications in low-power wireless systems, such as RFID systems [15, 16], wireless renewable sensor networks [17], body area networks [18, 14], and backscatter communication systems [19, 20, 21]. Additionally, RF-powered communications have a profound impact on the development of IoT [22] and machine-to-machine communications [23]. The readers referred to the recent survey in [24] for detailed overview of existing applications of RF-powered communications and envisioned future applications. For instance, in [25], a passive WuRx design operating at a frequency of 433 MHz is presented. The latter WuRx is powered through radio signals which trigger a wake-up interrupt when enough energy is harvested and stored. The authors design a WuRx that consists of zero-bias Schottky diodes acting as both a voltage multiplier and a radio trigger circuit. This WuRx also includes the addressing capability embodied in the WuS at different frequencies to activate only specific nodes, and it could reach a max distance of around 3m. The power consumption of this WuRx while harvesting energy from the transmitted signals is only $145\mu\text{W}$. The designed system was simulated and evaluated on SPICE [26]. Moreover, in [27], another WuRx operating at 900MHz consisting of a passive CMOS chip and an RF front end. The RF block consists of a rectifying circuit and a voltage multiplier and power management unit. The authors designed a 4-stage voltage multiplier using Schottky diodes. The power consumption of this WuRx is $2.64\mu\text{W}$. Also, [28], presented a passive 868MHz WuRx front end that harvests energy from RF signals. Here the RF radio blocks consist of an antenna, a matching network and a voltage multiplier. An RF-to-DC converter is used to convert the RF signal to a DC voltage that powers the sensor system. Donno et al. [29], designed a passive WuRx prototype using 868 MHz Ultra High Frequency (UHF) RFID tags and RFID energy harvesters to for achieving lengthy distances. Authors also developed a wake-up strategy called Enhanced Write Wake Up (E-WWU). The latter supports both broadcast communication and node addressing achieving maximum distance of 22m with transmission power of 30dBm. The WuRx side consumes $54\mu\text{W}$ when receiving the WuS.

Recent efforts focused on further increasing the power delivery efficiency. Thus, various prototypes have been proposed for RF energy harvesting. For example, [30] shows that an output DC voltage of 224 mV and an RF-to-DC conversion efficiency of 40% can be reached with the designed dual-band RF energy harvester for GSM-1800 and UMTS-2100 bands. Also in [31], ambient RF energy harvesting is tested on a novel six-band dual circular polarization (CP) rectenna. A public square is chosen to evaluate the rectenna as an outdoor ambient environment. The square is not in the line of sight of any high-power RF sources such as mobile base stations. The received ambient signal levels as

a function of frequency. For cellular mobile bands, the signal level in outdoor measurement is between -35 dBm to -25 dBm. Due to the limits of the Wi-Fi router distribution, the received Wi-Fi signals are only available at low levels around -37 dBm at the indoor environment. This rectennas overall measured conversion efficiency is up to 26% for the for a wide range of load between 10 and 75 k Ω . A dual band harvester is introduced in [32] for GSM 900 MHz and 1800 MHz bands. The efficiency of the proposed prototype is 40.8% and 20% at 1834 MHz and 890 MHz, respectively with an incident power of -20 dBm. The trial test shows that an excess of 0.5 V can be harvested from the environment without a source nearby. In [33] a triple-band harvester is proposed for ambient RF energy harvesting. The circuit operates at three frequency bands: GSM 1800, UMTS 2100 and LTE 2600, and can lead to a high RF-to-DC conversion efficiency that reaches 35% with an input power of -20dBm. From the voltage reading of 0.381 V and load RL of 5.6k Ω , the equivalent harvested power is approximately 25 μ W. The authors in [34] propose a broadband harvester that collects ambient RF energy over six frequency bands at the same time.

Although many of the WuR solutions proposed for WSN operate at cellular frequencies, the use of Wi-Fi solutions in wake-up and harvesting designs is gaining more attraction recently for the following key reasons:

- Wi-Fi is ubiquitous in indoor environments and operates in the ISM band where transmissions can be modified to deliver power. Utilizing Wi-Fi networks for power delivery and wake-up can ease the deployment of RF-powered devices without additional infrastructure.
- Given Wi-Fi's economies of scale, Wi-Fi chipsets provide a cheap platform for sending signals that can enable efficient power delivery [35].
- Sensors and mobile devices are increasingly equipped with antennas for communication via Wi-Fi, Bluetooth or ZigBee. We can, in principle, use the same antenna for both communication and Wi-Fi power harvesting with a negligible footprint on the size of the device [36].

Recently, researchers have explored the feasibility of harvesting RF power in the Wi-Fi 2.4 GHz bands [37, 38, 39, 40, 41]. However, these research efforts focus more on harvesting from continuous wave transmissions than from actual commercial Wi-Fi routers. Nonetheless, the transmission characteristics of the Wi-Fi traffic which is an alternation between continuous transmission and silent periods is the key reason that constrains the rectifier circuit and limits its rectification efficiency. In [38, 41], the authors design a rectifier that outputs a voltage of 100 mV from continuous transmissions at specific frequency tones. The work in [40] proposes a rectenna patch design at 2.4 GHz for battery charging purposes. The proposed design is evaluated with continuous transmissions in a specific anechoic chamber. A new group of RF energy harvesters, called waveform aware

harvesters is proposed in [42], where the impact of the bursty nature of Wi-Fi traffic on the efficiency of the rectifier is analyzed and studied. These rectifiers are optimized for their performance with non-continuous wave transmissions which constitutes a significant improvement in ambient energy harvesting. The work in [42] presents an initial proof-of-concept demonstration of a waveform aware harvester optimized for harvesting energy at 2.4 GHz from Wi-Fi (802.11b/g) signals with a realistic traffic model. It also provides an optimized recovery of harvested energy from single 802.11b/g transmission bursts on the order of 1 ms in duration.

In [39], the key challenges faced in harvesting from an actual Wi-Fi router are highlighted. There is a fundamental mismatch between the requirements for power delivery and the Wi-Fi protocol. The silent periods present during Wi-Fi transmissions limit the ability of the harvester in meeting a minimum voltage. Therefore, power over Wi-Fi (PoWi-Fi) is introduced as a solution for the imbalance between the demands of power delivery and the Wi-Fi protocol[39]. At a high level, a router running PoWi-Fi imitates a continuous transmission while minimizing the impact on Wi-Fi performance. Basically, PoWi-Fi injects UDP packets on multiple channels on the MAC layer achieving continuity but limits the users in the network and adds complexity and payload overhead to these users. According to [39], a PoWi-Fi router utilizes three Atheros AR9580 chipsets that independently run an algorithm on channels 1, 6 and 11. Each chipset is connected to a 6dBi Wi-Fi antenna through amplifiers. The designed prototype router provides both internet access associated clients and with a transmit power of 30dBm. However, the Atheros chipsets integrated with the antennas modify the router's topology and hardware.

Chapter 3

RF Energy Harvesting from Ambient Wi-Fi Signals

3.1 System Model and Definitions

In this chapter, the system for ambient RF energy harvesting is presented. The system consists of a front end circuit that can harvest energy from RF signals and use this energy to activate a compact device. The power consumption of the harvesting circuit must be extremely low in order not to affect the energy efficiency of the device it is powering. An RF energy harvesting system is composed mainly of a rectenna system that is cascaded with a power management unit. The antenna receives the ambient RF energy and this harvested energy is rectified, filtered and stored in a specific rechargeable battery or a super capacitor. After a given time, this storage component can supply large enough power levels that are needed to operate the IoT device. In addition, the needed energy can be reduced by implementing a wake-up protocol. In this case, the harvested energy is not stored, but rather directly used to trigger the IoT device from the sleep mode to the active mode where it uses its original battery. A diagram of an RF wake-up device is presented in Fig. 3.1. A comparator connected to an active power source is used in the RF wake-up circuit to step the low voltage at the output of the rectifier to a higher level capable of triggering the main microcontroller of the IoT device and switch it to the active state. Fig. 3.2 shows an RF powered device where a DC-DC converter is used along with an energy storage unit to collect sufficient amount of energy to power the microcontroller and other components of the circuit.

3.2 Challenges of Harvesting Wi-Fi Signals

Fundamentally, the majority of the proposed work in the literature focus on harvesting from dedicated point-to-point transmissions at 2.4 GHz. Such focus

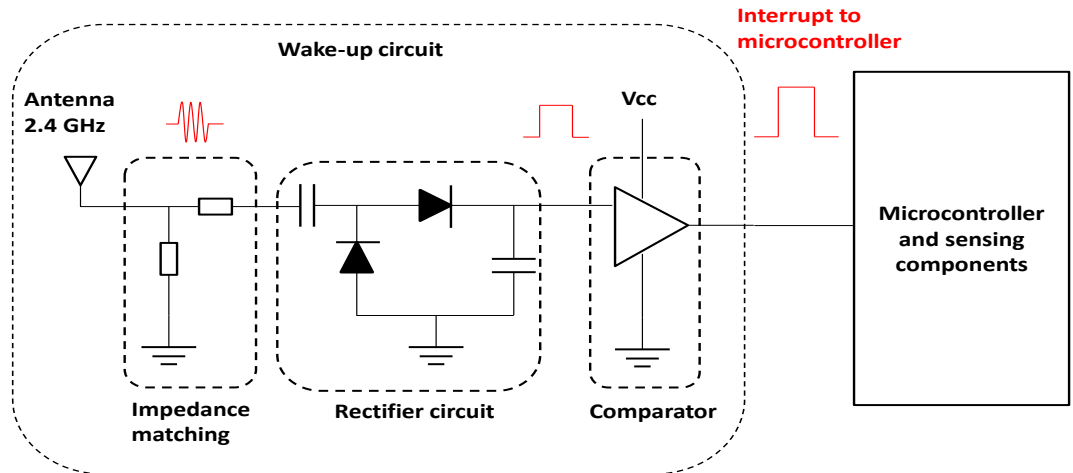


Figure 3.1: Block diagram of an RF wake-up device.

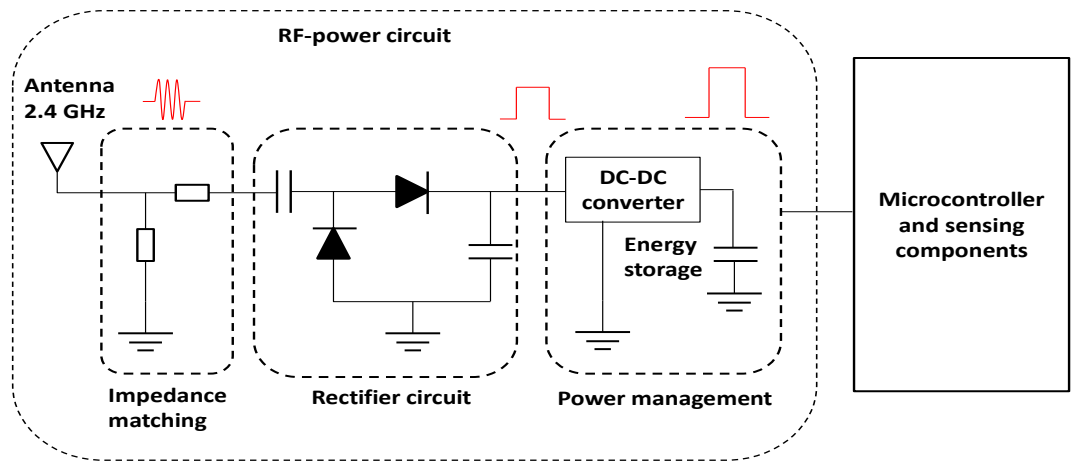


Figure 3.2: Block diagrams of an RF powered device.

on dedicated transmitters can dismiss the challenges that typically accompany energy harvesting from real ambient sources. Therefore, in order to spot the difference between ambient and dedicated transmissions, we placed a 2.4 GHz rectifier circuit 50 cm from an RF signal generator for the dedicated transmission, and later from a commercial router for ambient transmission. We measure the output DC voltage for the two considered scenarios. An output voltage of 0.398 V was collected from the dedicated transmission, while only 22 mV resulted when harvesting ambient Wi-Fi signals.

Basically, the power leaks during silent periods and significantly limits the Wi-Fi's ability to meet the minimum voltage requirement of the considered application. Fig. 3.3 illustrates the router's performance and its burst signals. The

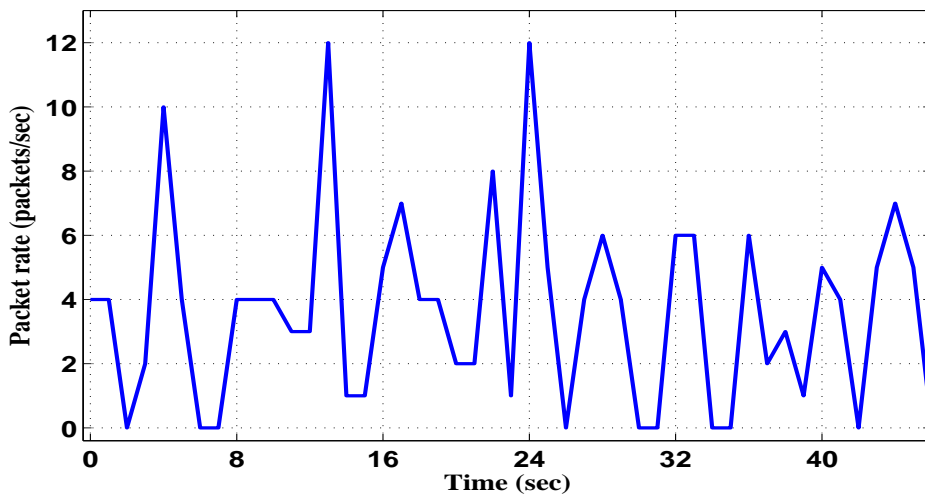


Figure 3.3: Router’s normal activity.

nature of the Wi-Fi’s signals are inherent to a distributed medium access protocol that is based on the alternation between continuous and silent transmission periods [35]. Therefore, obtaining a signal that could be rectified from commercial routers to wake up and recharge sensors efficiently, is the main motivation behind this work.

In order to quantify the difference between ambient and dedicated transmissions, we utilized an antenna that harvests the ambient electromagnetic energy and a rectifier that converts this signal to DC. The rectifier circuit is designed on a Rogers 3202 substrate with a thickness of 0.508 mm and dielectric constant of 3.02. The rectifier’s dimensions are 32.21 mm x 17.54 mm. A commercial TL-WR541G 54 Mbps Extended Range router is used [43] to transmit RF signals to the rectifier circuit. The router’s antenna is omni-directional and has a gain of 3 dBi [43]. In order to gain control over the power transmitted, bandwidth, and channels of the router, the DD-WRT software is used [44]. DD-WRT is a Linux-based open source firmware that facilitates the manipulation of the router’s parameters and specifications. The router offers transmit powers that range from 0 dBm to 17 dBm. It covers the first 11 Wi-Fi channels (2.412 – 2.462 GHz). The bandwidth can be set to either 5, 10, 20 or 40 MHz. We then run an experiment where a rectifier that operates at 2.4 GHz is positioned 50 cm away from an RF signal generator. The signal generator is connected to an appropriate antenna that ensures dedicated continuous transmission. Later on, the same circuit is placed 50 cm away from a commercial Wi-Fi TL-WR541G router for ambient transmission. The output DC voltage is measured in both scenarios. An output voltage at a load of 1k Ω is 398 mV from the dedicated transmission, while only 22 mV are captured when harvesting from commercial ambient Wi-Fi signals.

3.3 Software Based Router Data Transmission

In this section, we explain the novelty of the proposed software-based algorithm for energy harvesting using Wi-Fi data transmission, and we highlight the effectiveness of this design.

As shown in Fig. 3.3, the router sends intermittent signals which make harvesting very difficult. Basically, we can notice from Fig. 3.3 that when there are packets sent over the network, a peak is observed. Therefore, to achieve a continuous peak, additional traffic should be introduced. As a result, artificial packets can be built and sent over the network to enforce high Wi-Fi channel occupancy. These artificial packets are built using Colasoft Packet Builder [45]. The benefit of employing such a technique is based on the fact that no additional external hardware or component is needed, in addition to the fact that such technique can be applied to existing commercial routers. At a high level, the designed system injects Ethernet II broadcast packets [46] with the highest Wi-Fi rate to deliver power on the designed Wi-Fi channel. The Colasoft software helps in customizing the packets sent as desired. The injected packets contain only the source address, the destination address, the length/type field and the frame check sequence (FCS). The source address is the laptop that has the Colasoft software installed.

The antenna captures all the signals because all the router transmissions, either data or dummy packets, are more or less the same. As a result, through the packet injection technique, the rectifier is able to identify an almost continuous Wi-Fi signal. Such identification enables the harvester to operate at full efficiency since virtually the problem of non-continuity and intermittent nature of the Wi-Fi signal is solved. Fig. 3.4 presents the router's normal activity and the router's activity when the proposed packet injection algorithm is applied. The algorithm targets the physical layer messages. Hence, the router continues its natural performance while harvesting energy. When the algorithm is running, the average packet rate increases as shown in Fig. 3.4. In these results, the packet size chosen is 1000B.

3.3.1 Ambient Vs. Dedicated Transmission

In this section, we compare the dedicated transmission scenario with the scenario when the proposed packet injection algorithm is implemented on a commercial router. Fig. 3.5 illustrates the ambient RF energy harvesting setup. The router is placed at a distance of 50 cm (far field region) facing the receiving rectenna system. At this distance the power received varies between -23 and -5 dBm after transmitting at a power level between 0 and 17 dBm. For the dedicated RF energy harvesting setup and in order to mimic the ambient setup, the monopole is detached from the router and connected to a dedicated RF source for the same distance and power transmitted. From each experiment, the voltage results are

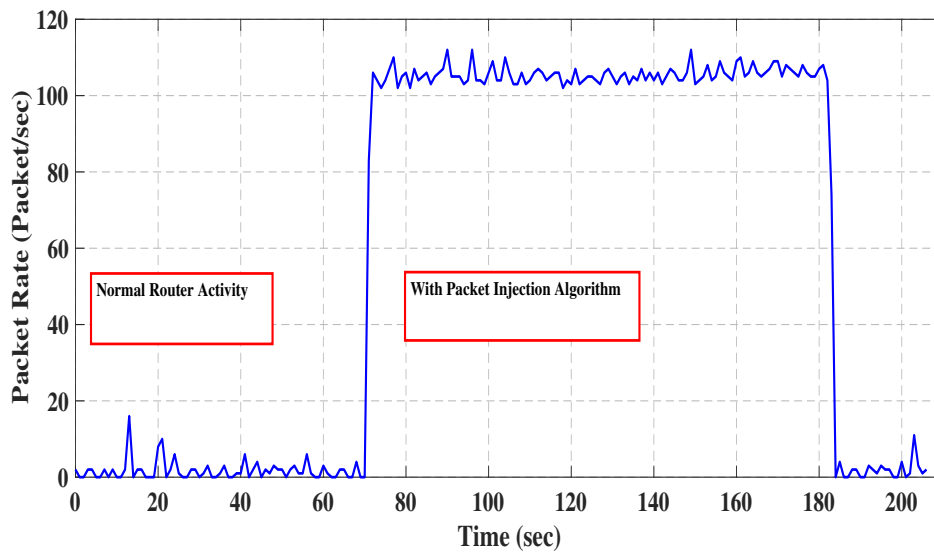


Figure 3.4: Router's packet rate with and without packet injection.

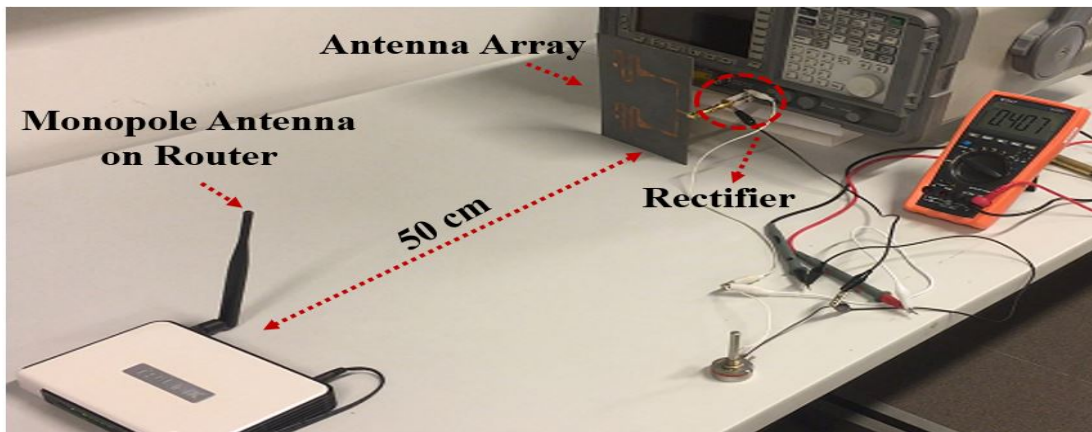


Figure 3.5: Ambient harvesting setup.

extracted at a load of $1\text{ K}\Omega$, at channel 3 (2.422 GHz). The efficiency is then calculated and plotted in Fig. 3.7. This figure shows an agreement between the efficiency results of harvesting from a dedicated RF source and from an ambient source. The harvester is now able to rectify signals that are arising from an ambient wireless router with a very similar efficiency to the dedicated signals scenario. The resulting efficiency values are also very close to the ideal scenario shown in Fig. 3.8 where voltage results are extracted by directly connecting the rectifier to the RF signal generator.

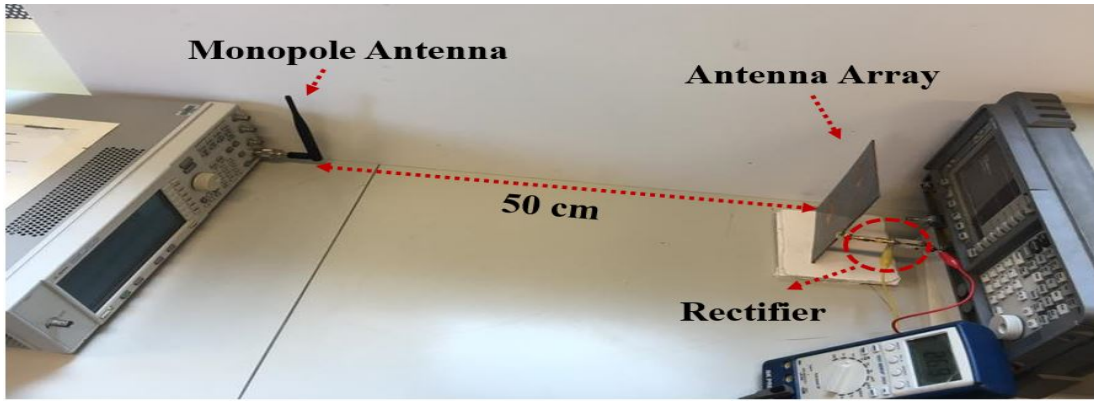


Figure 3.6: Dedicated harvesting setup.

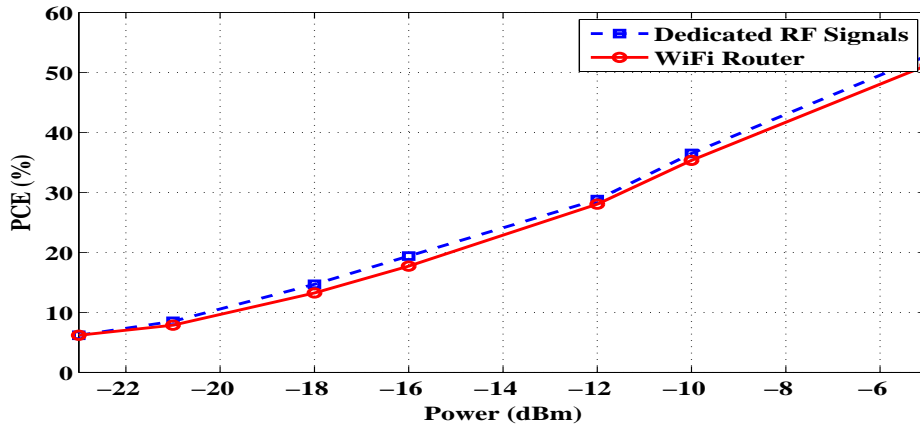


Figure 3.7: Efficiency comparison between dedicated and ambient scenarios.

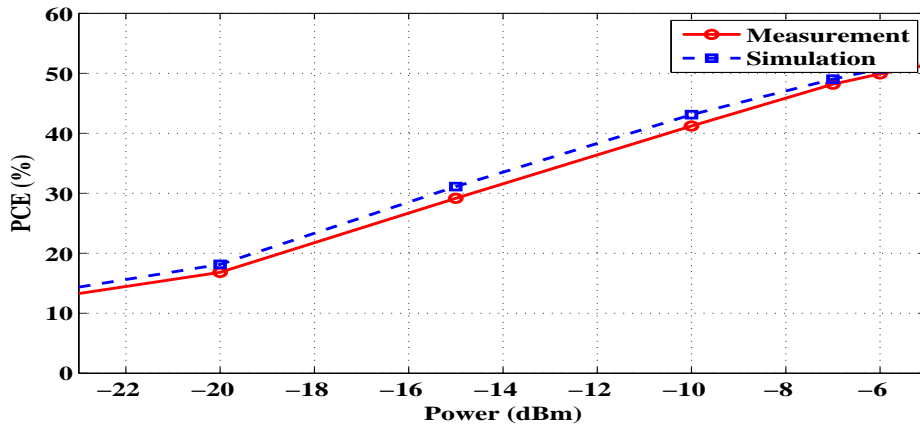


Figure 3.8: Efficiency results for the rectifier with proposed matching technique.

3.3.2 Efficiency Response With Respect To Wi-Fi Channels

The tapering technique implemented in the rectifier circuit forces it to have a smooth almost flat efficiency response across all Wi-Fi channels. The setup presented in Fig. 3.5 is repeated while sweeping the frequency from channel 1 to channel 11. For a transmitted power set to 10, 12, and 17 dBm at a distance of 50 cm, the expected received power levels are -12, -10, and -5 dBm respectively. This corresponds to around 29%, 37% and 50% power conversion efficiency respectively as presented in Fig. 3.9. The rectifier also presents a stable efficiency response at all power levels along the Wi-Fi band.

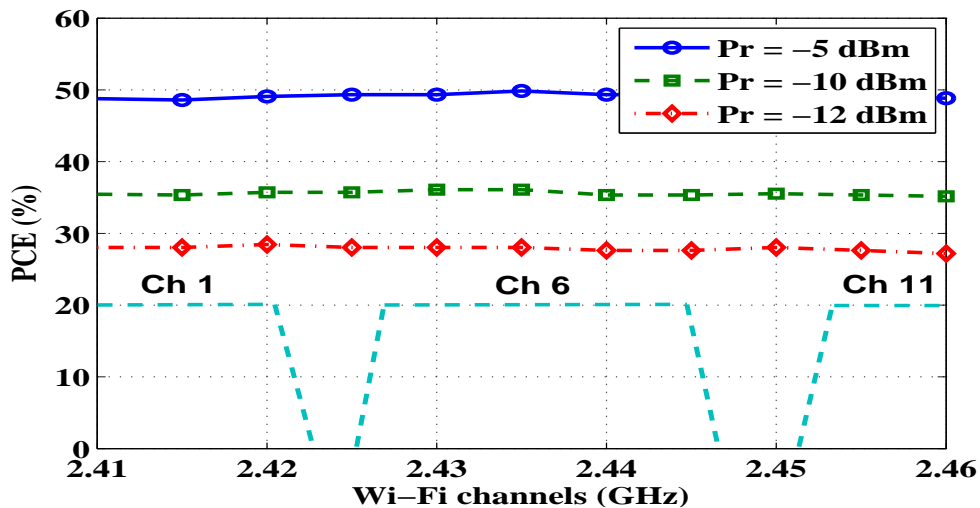


Figure 3.9: Measured PCE results with respect to frequency for different received power levels.

3.3.3 Efficiency Response With Respect To Distance

In this section, the rectifier is evaluated for its ability to harvest from wireless routers at its threshold distance. The power transmitted from the router is fixed to 17 dBm while its position is swept between 50 cm and 420 cm. The lower bound denotes the beginning of the far field region while the upper bound represents the sensitivity level of the Schottky diode. At these two limits the power received is -5 and -30 dBm respectively. Fig. 3.10 shows the variation of the received power and the efficiency with respect to distance. For the same transmitted power, the received power decreases with distance which leads to a fall in the efficiency from 50.52% to 2.6%. This experiment shows that the rectifier is able to harvest up to a distance of 420 cm. This relates to the Schottky diode sensitivity limitation described in details in [47, 48].

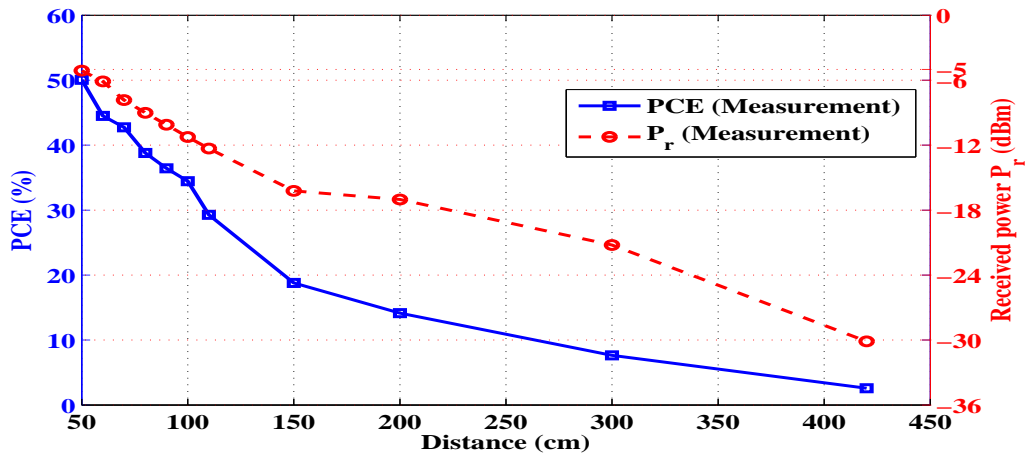


Figure 3.10: Measured PCE and received power results with respect to distance.

3.4 Effect on Active Wi-Fi Users

3.4.1 System Overview and Parameter Definitions

The packet injection algorithm is designed to maximize the efficiency of power delivery, which is translated in an increase in the channel occupancy. A straightforward solution is to transmit large sized packets continuously. This approach however, deteriorates significantly the Wi-Fi router's performance and adds traffic to the network. Therefore, the appropriate packet size should be optimized in such a way will not result in denial of service (DoS). The latter is an attack on the network that preserves all the resources and makes them unavailable to the intended users in the same network. Thus, the notion of inter-packet delay is introduced as an important parameter to avoid DoS problems.

Therefore, in order to study the effect of the packet injection algorithm on other users, an experiment is conducted with four Samsung S4 devices. These devices are designated as users that stream a video of size 16.81 Mbytes each. An application called "CoCodi" is installed on all of these devices. Such mobile application measures the user's bit rate, duration, packet success rate (PSR) and packet received ratio (PRR). The PSR is the percentage of packets that are successfully transmitted while downloading a video. The PRR gives the percentage of the number of nodes that received the tagged packet successfully before it expires. Notice that in this experiment, the Wi-Fi router is configured to transmit on only channel 3.

In order to have a fair comparison, several tests are conducted. First, the four S4 devices stream the video simultaneously. The average achieved bit rate and duration are equal to 0.85 Mbps and 2.05 min respectively. For this case, the PSR=89.975% and the PRR=90.01%. Thus, the higher the value of PSR and PRR, the better is the network performance.

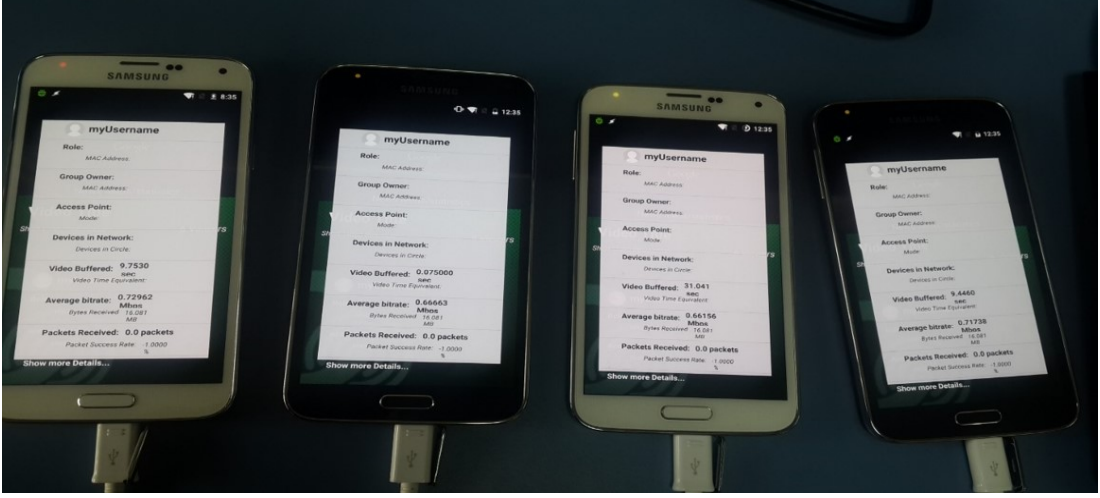


Figure 3.11: Samsung S4 devices streaming data from the Wi-Fi access point.

Next, the packet injection algorithm is enabled and different packet sizes and inter-packet delays are considered. However, we need to find the best packet size and inter-packet delay values that will have a minimal effect on the network. In principle, having a large packet limits users in the network to transmit because Wi-Fi is based on Carrier Sense Multiple Access collision avoidance (CSMA/CA) [35] where a user can only transmit if it senses that no one is using the channel. Furthermore, transmitting large packet sizes will lead to memory size restrictions. The larger the packet size, the higher the probability that it will get dropped or in worst cases to get fragmented. If this is the case, retransmission is bound to occur. Thus, this will lead to a higher channel occupancy and will cause the retransmission timeout (RTO) to increase. The packet injection algorithm is designed to increase channel occupancy and to achieve continuous superfluous transmission so that the rectenna system can harvest the signals efficiently. Hence, packet size is an important parameter which impacts throughput, delay, packet-drop probability and efficiency.

Theoretically, if the packet size and the inter-packet delay increase, the number of packets sent will decrease. For a link layer speed of 65Mbps the number of packets sent over 10s is plotted using (3.1) and (3.2), where L is the link layer speed converted to MBps, the duration is D and the inter-packet delay is denoted at IDY . The number of packets sent in 10s is denoted as NP . We notice in Fig. 3.12, if we decrease the packet size and the inter-packet delay, the more the packets that are sent.

$$D = \frac{PS}{L} + IDY \quad (3.1)$$

$$NP = \frac{10}{D} \quad (3.2)$$

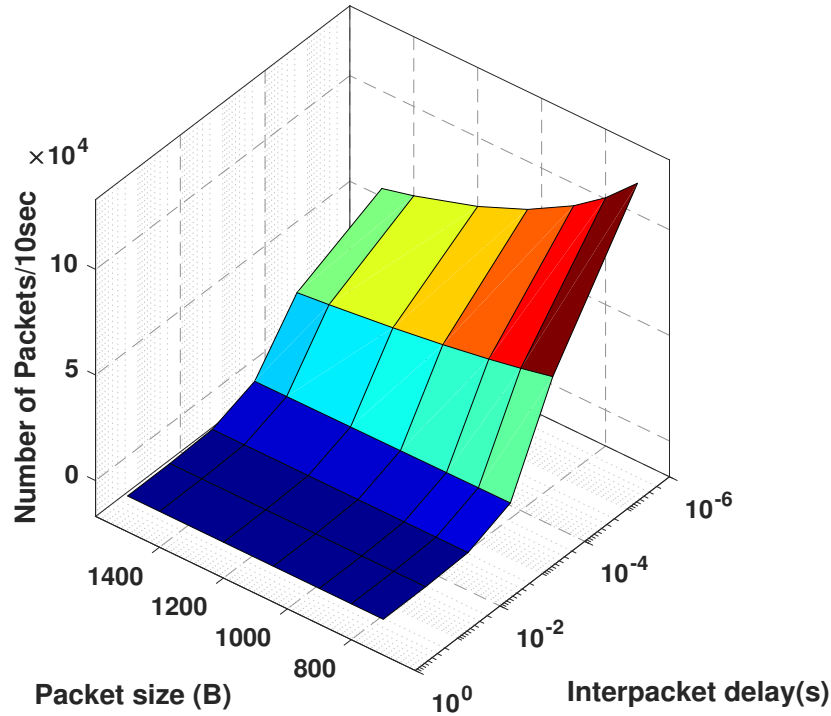


Figure 3.12: Number of packets sent over a period of 10sec while varying the packet size and interpacket delay.

3.4.2 Efficiency and Network Performance

In order to visualize the effect of the packet size and inter-packet delay on efficiency and channel occupancy, we measured the number of packets sent using wireshark for each packet size as we vary the inter-packet delay. Accordingly, we choose packet sizes that range between 700B and 1500B with inter-packet delays of 0s to 0.1s. From Fig. 3.13, 3.14 and 3.15, we can conclude that if we increase the packet size the efficiency of the rectenna system will increase.

However, with larger packet sizes we are using most of the resources in the network. Consequently, if we use smaller packet sizes, the network can be occupied by other users; however, the efficiency level decreases. To avoid congestion problems, we increase the inter-packet delay duration. For a higher inter-packet delay, the continuity is almost lost and the efficiency drops dramatically at an inter-packet delay of 0.1s. Hence, a compromise must be made between achieving high efficiency and maintaining a minimum effect on the users in the network. We also measured the variations in the PSR and the PRR on the "CoCodi" application for different packet sizes and inter-packet delays. Fig. 3.16 and 3.17 show that if we increase the packet size the PSR and the PRR values will decrease. For example in Fig. 3.16, for a packet size of 700B and 0s inter-packet delay the PSR

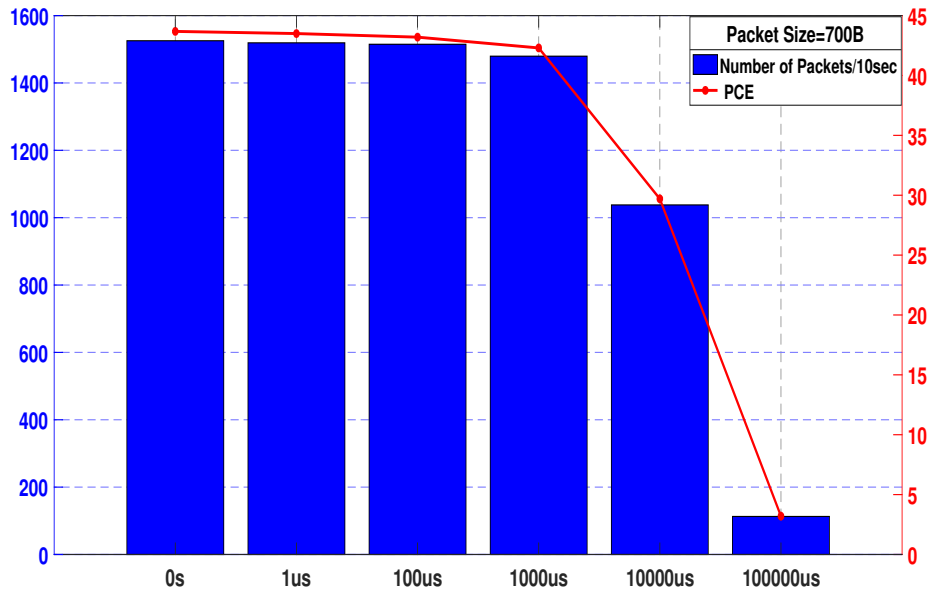


Figure 3.13: Number of packets sent and efficiency for a packet size of 700B over different inter-packet delay duration.

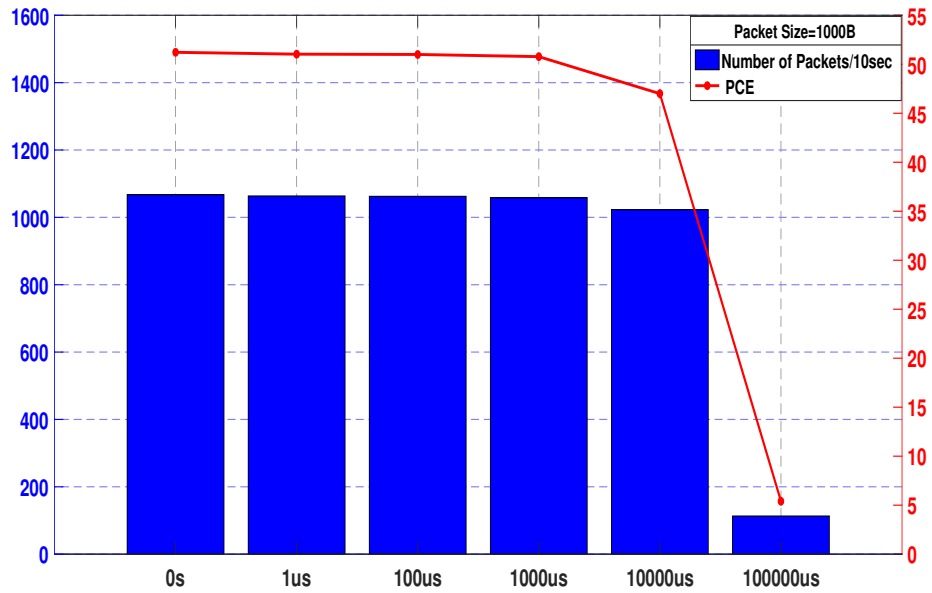


Figure 3.14: Number of packets sent and efficiency for a packet size of 1000B over different inter-packet delay duration.

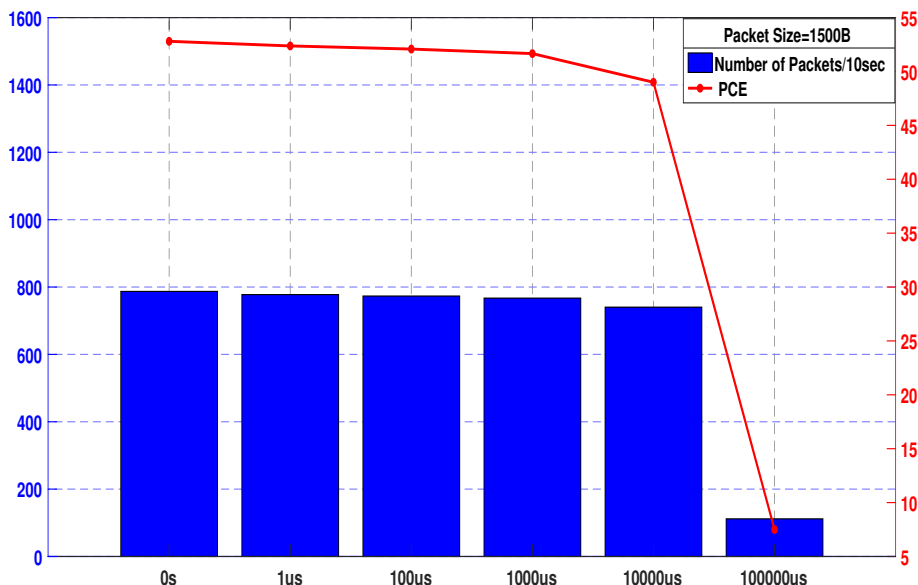


Figure 3.15: Number of packets sent and efficiency for a packet size of 1500B over different inter-packet delay duration.

level is 73.086%. But if we increase the packet size to 1500 with 0s inter-packet delay, the PSR value is 66%. The decrease in the PSR value will deteriorate the performance of the network. However, if we increased the inter-packet delay, the PSR and the PRR values will increase accordingly. Consequently, we choose a packet size and an inter-packet delay that will achieve a high antenna efficiency and provide sufficient resources for others users in the network. Therefore, we tentatively choose a packet size of 1000B and an inter-packet delay of 1ms inter-packet delay. Furthermore, we need to validate the effect of the chosen parameters on an actual real time scenario. Therefore, we run the same experiment as before where four Samsung devices stream a live video. The bit rate and the download duration is measured for different packet sizes inter-packet delay. The voltage received levels that reflect efficiency are also plotted. Fig. 3.18 presents the average download duration and the DC voltage at the output of the rectifier with a fixed inter-packet delay of 1 msec for different values of the injected packet size. A clear trade-off can be noticed; when the packet size increases, the rectified voltage level increases which corresponds to a higher efficiency. However, the video takes a longer time to be downloaded and thus, the quality of service of the Wi-Fi users deteriorates. Similarly, the download bit rate decreases when the packet size increases Fig. 3.19.

Another parameter that is studied is the inter-packet delay. In the previous experiments, we fixed the inter-packet delay to 1 msec. For this case, the packet size is fixed at 1000 bytes and different inter-packet delay values are considered. Fig. 3.20 and Fig. 3.21 present the average bit rate and download duration in

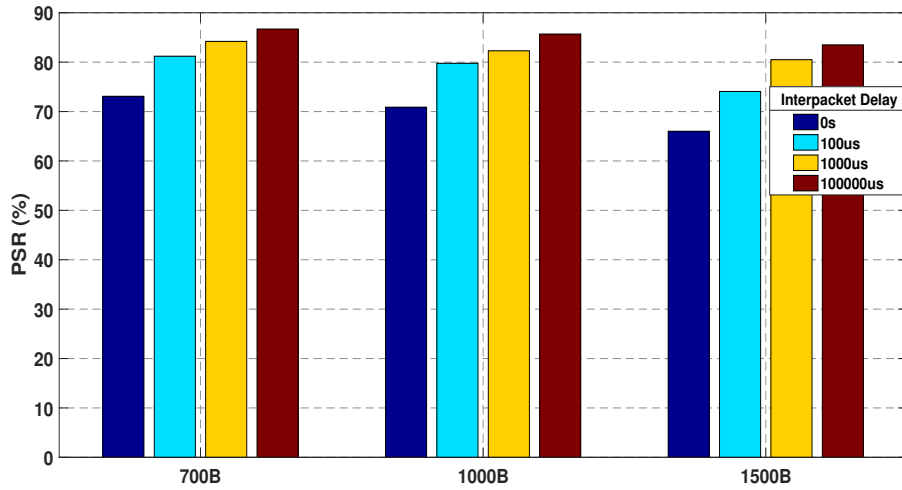


Figure 3.16: Packet Success Ratio.

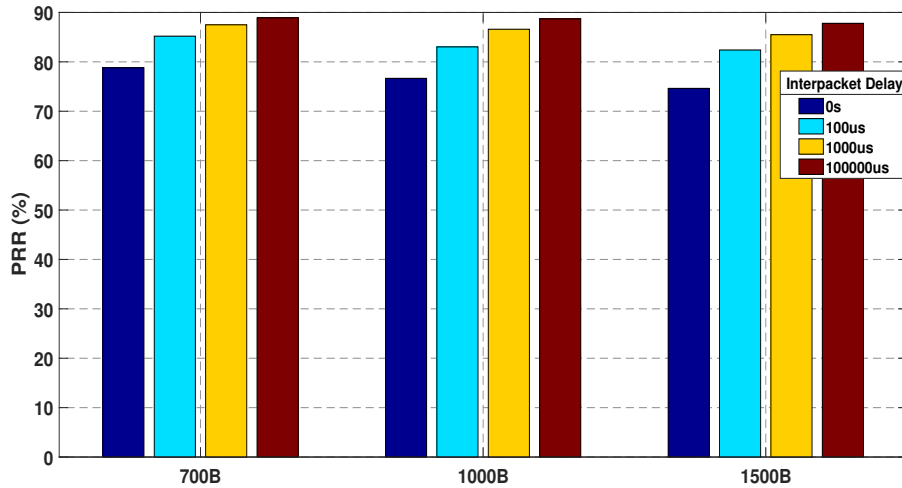


Figure 3.17: Packet Received Ratio.

addition to the DC voltage as function of the inter-packet delay. From these figures, we can notice that, as the inter-packet delay increases, the average bit rate increases and the download duration decreases. However, the obtained DC voltage decreases slowly until the inter-packet delay exceeds 10 msec. Thus, the efficiency of power delivery can be almost conserved while maintaining an acceptable level of performance for the Wi-Fi users.

Accordingly, the packet injection algorithm is optimized such that the size of the injected packets is 1000 bytes and the inter-packet delay is 1 msec, which leads to an efficiency of 47.15% and a voltage level of 386 mV at a distance of 50 cm. The streaming duration in the considered scenario is 2.20 min and the bit rate is 0.805 Mbps. As a summary, when using the packet injection algorithm, the download duration increased by 8.1% and the bit rate decreased by 5.1%.

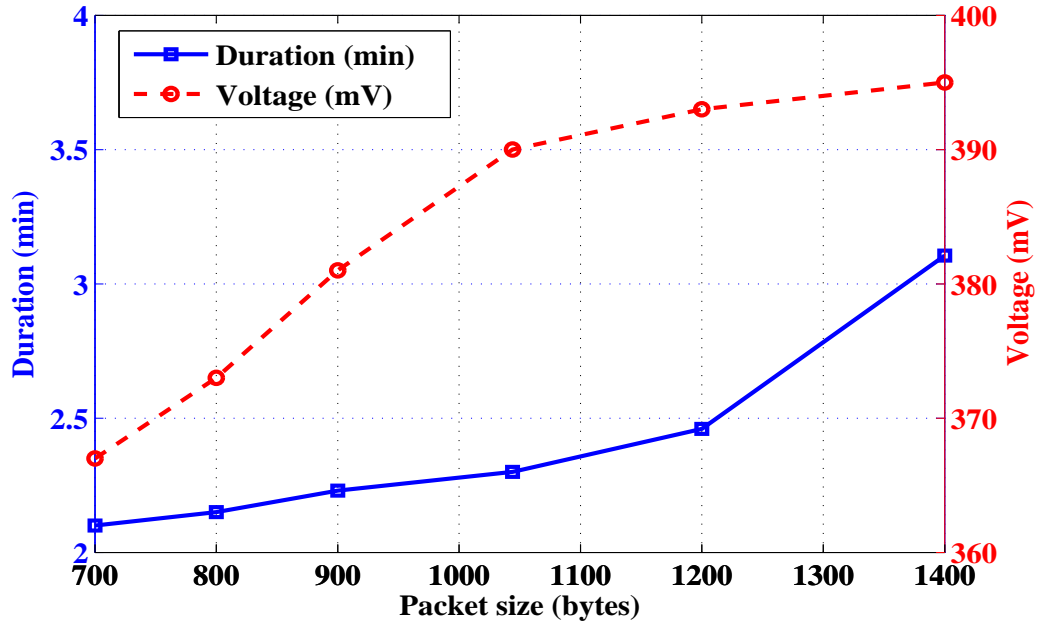


Figure 3.18: Download duration and DC voltage as function of the packet size.

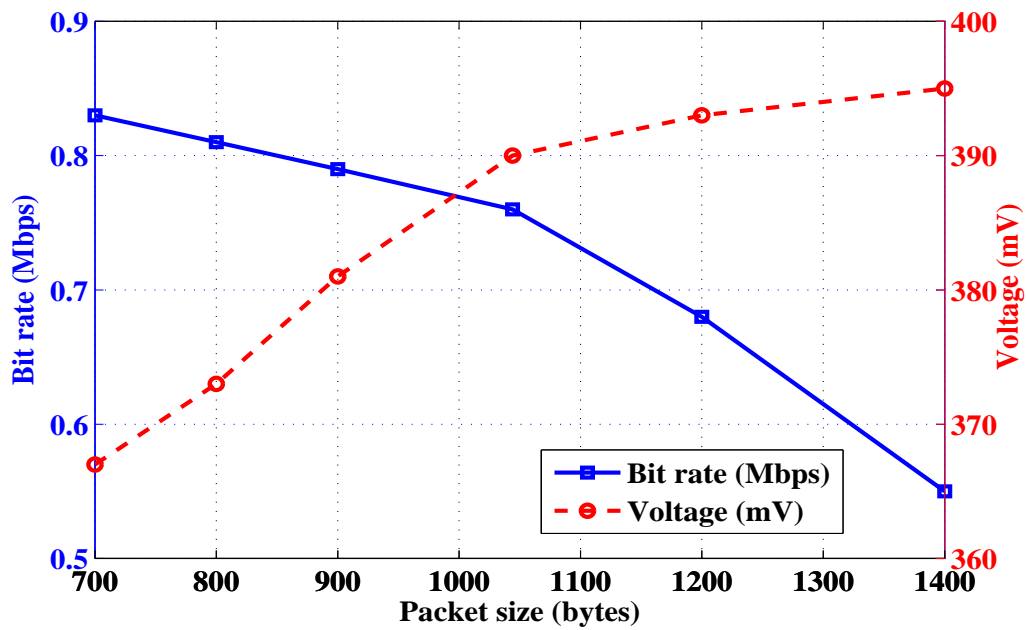


Figure 3.19: Download bit rate and DC voltage as function of the packet size.

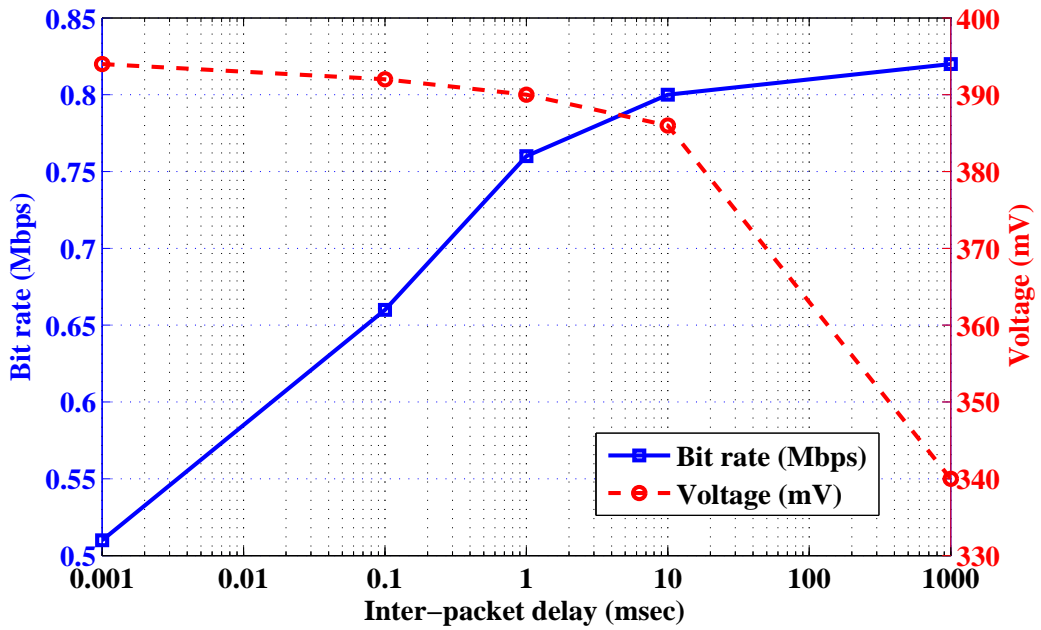


Figure 3.20: Download bit rate and DC voltage as function of the inter-packet delay.

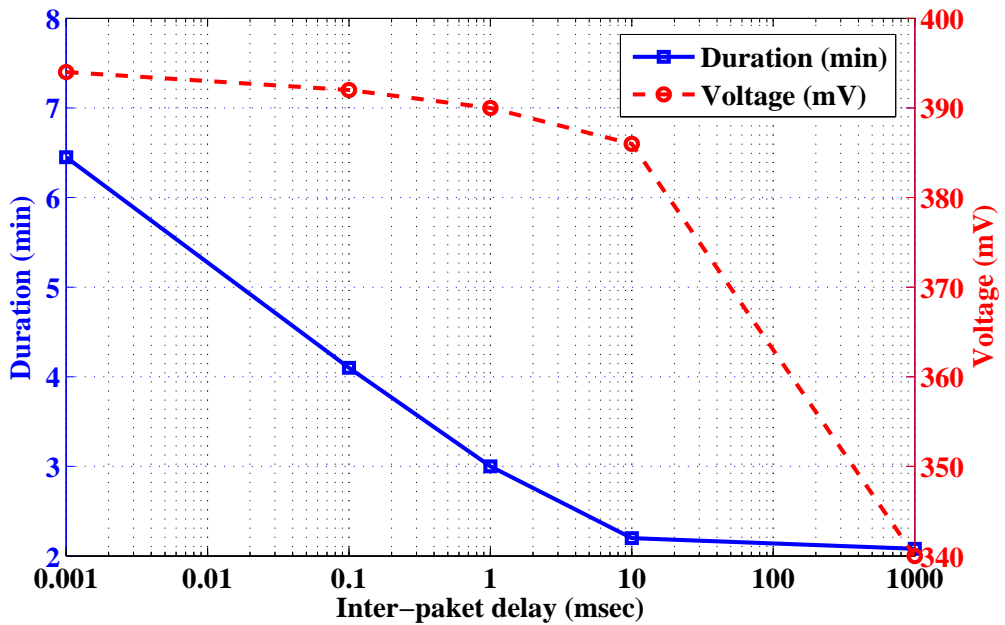


Figure 3.21: Download duration and DC voltage as function of the inter-packet delay.

Chapter 4

Positive Effect of Interference

Fig. 4.1 presents the proposed system model where Wi-Fi routers are exchanging data with sensor nodes and also waking up and charging IoT devices in their vicinity. We can notice that having multiple routers transmitting signals can cause many reflections and multi-path propagation. As a result, the router's signals will interfere with one another and either lead to a constructive signal or a destructive signal. For self-sustainable IoT networks, the interference caused by

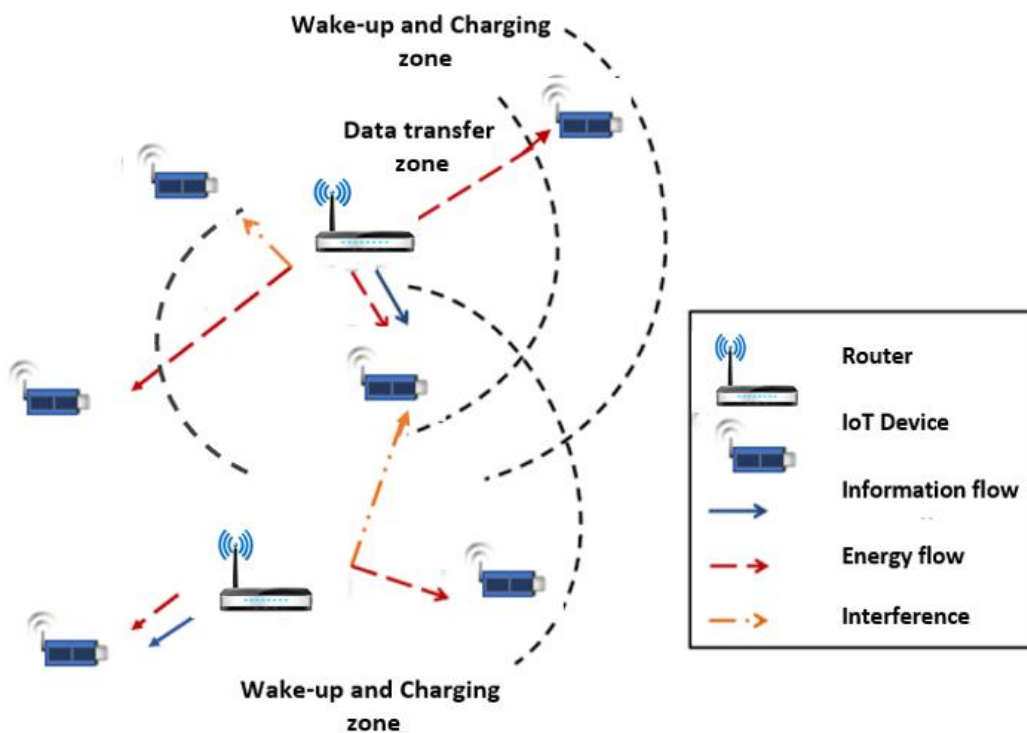


Figure 4.1: System model.

the transmission of ambient Wi-Fi routers may impair the capacity of communication. However, in this chapter, we will study the impact of capturing these signals on the Pr level. To highlight the effect of interference, the RF signals that emanate from Wi-Fi routers must be analyzed to evaluate their impact on the networks performance. Therefore, three different setups consisting of 3 Access Points (APs) are presented in this chapter. In each setup, the Pr level is captured using either a meandered line antenna of or an omnidirectional antenna. A comparative study that includes distance and antenna gain trade-offs along with the positive effect of interference is presented.

4.1 Experimental Setup

For the this experiment, 3 APs are placed in different positions. The basic setup is in Fig. 4.2. We place a spectrum analyzer to monitor the Pr level. In the previous chapters, we usually place the rectenna system at the receiving end rather than the spectrum analyzer. However, since we want the exact Pr level, we used a spectrum analyzer. Basically, we want to study the effect of interference from having additional APs. Therefore, as a starting point, we placed the APs at a 50cm distance from the spectrum analyzer until we reach a maximum distance of 200cm. The distance of separation between the routers vary from 50cm to 200cm for the first setup. For the second setup, the routers are next to each other while for the third, they are behind each other. In order to study the impact of each AP, we did the following: Turn one AP on and measure the Pr level, then turn another AP on and check the Pr level when both APs are on and then study the

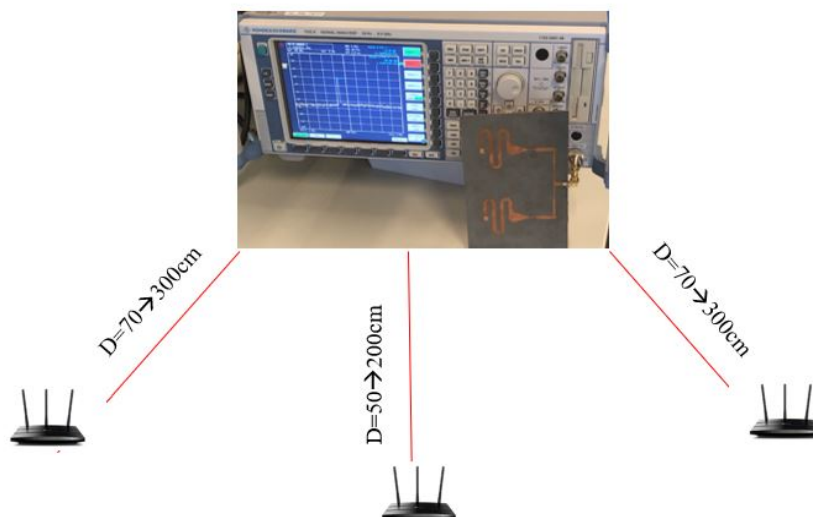


Figure 4.2: Effect of interference setup.

case when all of them are on. Hence, we have 8 combinations and 8 different Pr levels. However, we disregard the case when all APs are off.

The antennas polarization and gain play a major role in any Tx and Rx scenario. Specifically, in this setup, we start to examine the Pr level using a meandered line antenna that is placed at the receiver end. The meandered line antenna is a highly directive antenna with a 12.56dBi gain. It is a 2x1 antenna array and it operates at 2.45GHz. The meandered line antenna along with its radiation patten are shown in Figs . 4.3 and 4.4, respectively.

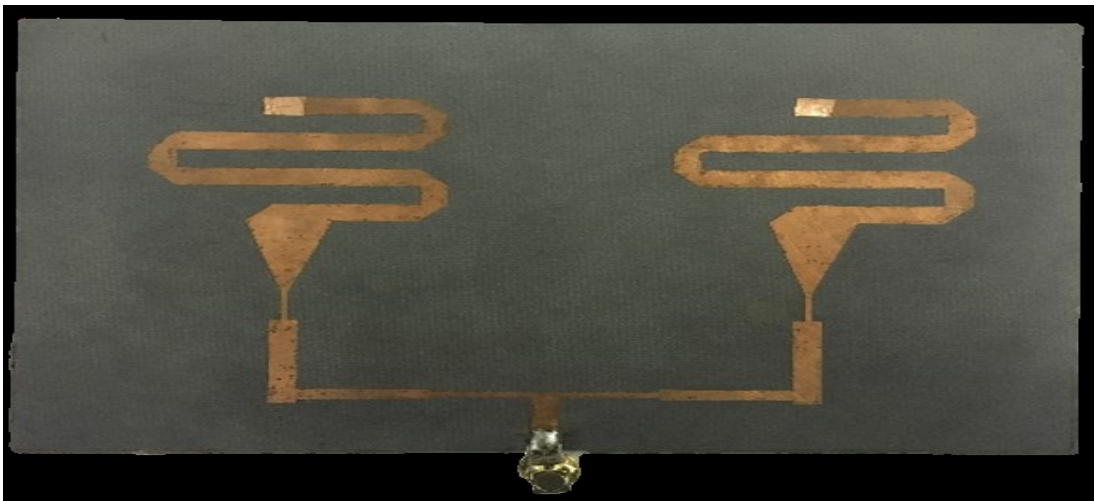


Figure 4.3: 2x1 meandered line antenna array.

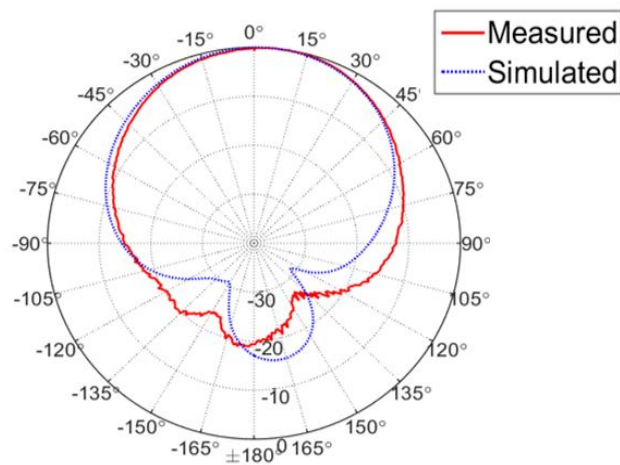


Figure 4.4: Meandered line antenna's radiation pattern.

However, the main drawback of the meandered line antenna is that its gain drops significantly if the transmitter and the receiver aren't placed in a perfect line of sight (LOS) manner. Furthermore, for the same setup as before, we replace the meandered line antenna with an omnidirectional antenna at the receiver's end. Fig. 4.5 shows the omnidirectional antenna that has a 3dBi gain. This antenna is linearly polarized but it is not as directive as the meandered line antenna array. Nonetheless, it doesn't have the dramatic P_r level drop if the Tx and Rx were not placed in a LOS manner. The radiation pattern of this antenna is shown in Fig. 4.6



Figure 4.5: Omnidirectional antenna.

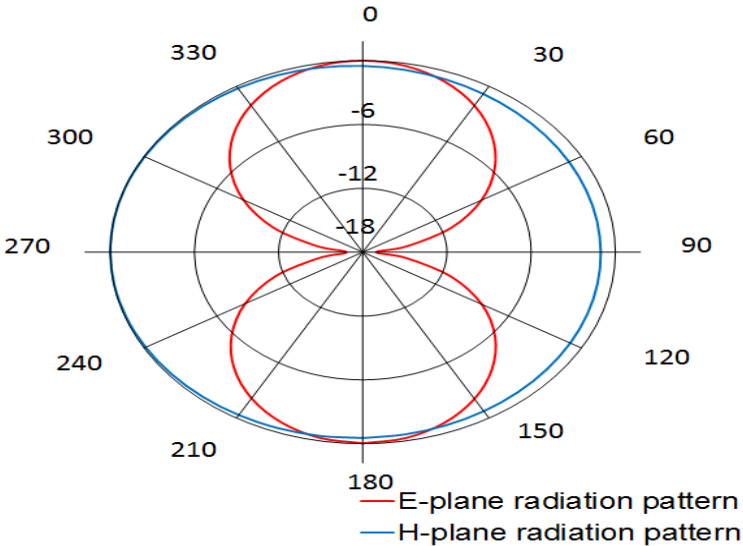


Figure 4.6: Omnidirectional antenna's radiation pattern.

4.1.1 Setup 1: Three APs at Various Distances

For the first experiment, 3 APs are placed at different distances from each other and from the spectrum analyzer. An antenna connected to the spectrum analyzer captures the transmitted signals and measures the power received levels. For the first setup, the distance of separation varies from 50cm to 200cm as illustrated in Fig. 4.7. In Fig. 4.8 the measured power received levels are plotted with respect to distance. We can notice that if we use a meandered line antenna the Pr level is higher because the antenna's gain is higher. Moreover, when all APs are on, a higher Pr level is captured by the antenna which illustrates the positive effect of interference.

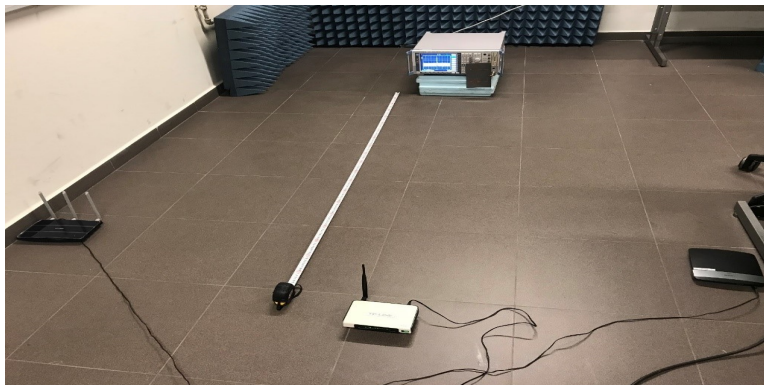


Figure 4.7: Experimental setup 1: Monitoring the Pr level from 3 APs placed at different distances from one another.

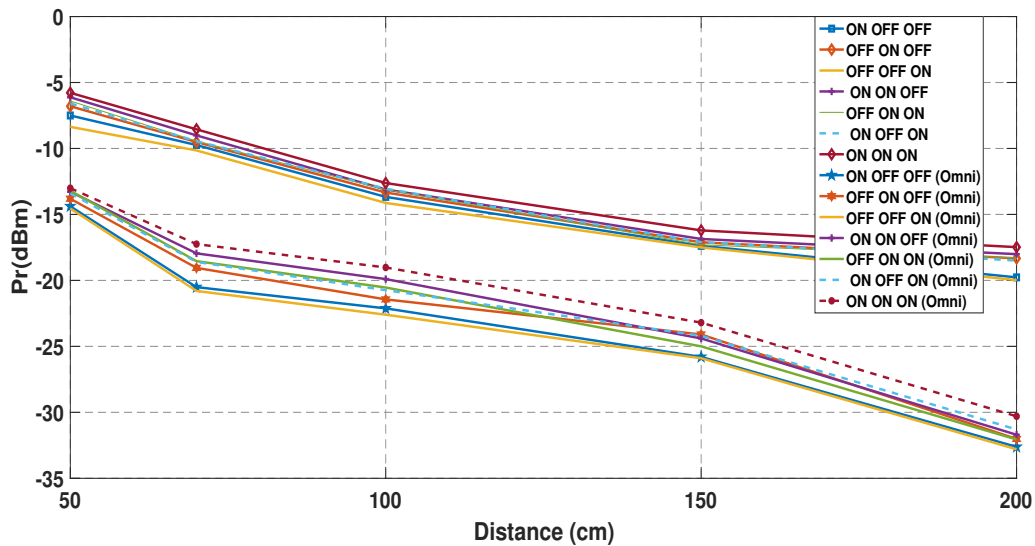


Figure 4.8: Results of setup 1: Pr on meander vs. omnidirectional antenna from 3 APs at different distances.

4.1.2 Setup 2: Three APs Next to Each Other

The next experiment is similar to the previous; however, the distance of separation between the routers themselves doesn't change. The distance from the antenna to the routers only increases from 50cm to 200cm. Now we have 7 different on-off combinations for the 3APs. Moreover, in this experiment also we compare the Pr level when a meandered line antenna is used to that of an omnidirectional antenna. Furthermore, Fig. 4.10 illustrates the Pr behavior of the second setup. We notice that the Pr level, when either a meander line antenna or an omnidirectional antenna are placed at the receiver's end, is slightly higher than the case when the routers were placed at different distances. Having this kind of setup seems to add the signals constructively because we obtain a higher Pr level at the spectrum analyzer.



Figure 4.9: Experimental setup 2: Monitoring the Pr level from 3 APs placed next to each other.

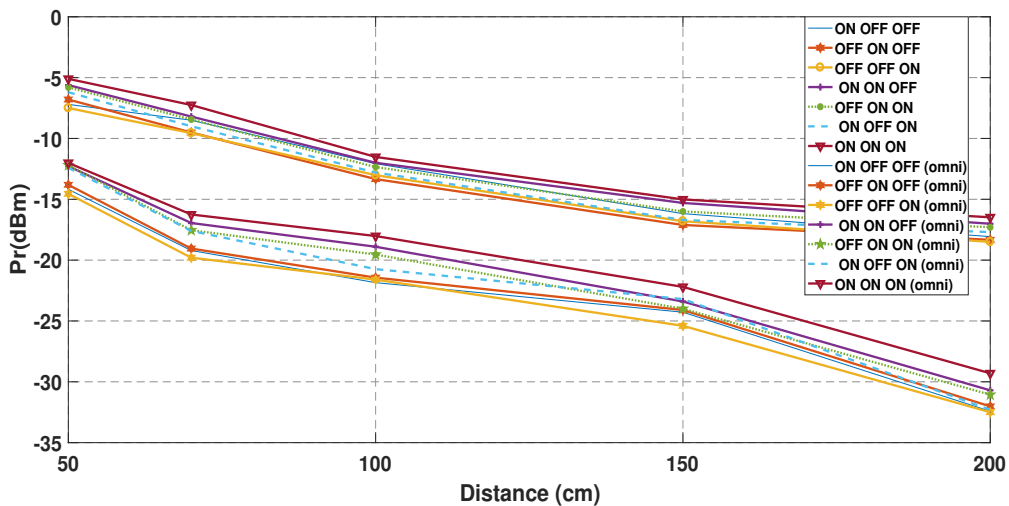


Figure 4.10: Results of setup 2: Pr on meander vs. omnidirectional antenna from 3 APs placed next to each other.

4.1.3 Setup 3: Three APs Behind Each Other

For this setup, since all 3 APs are directed toward the antenna, higher power is expected at the receivers front end. The setup here is similar to the previous experiments in terms of changing the type of antenna used and varying the distance. Again, different on–off combinations of the 3 APs are conducted in order to measure the Pr level. Setup 3 is presented in Fig. 4.11. For this setup, the results are shown in Fig. 4.12. We notice that the Pr level here is even higher than that of setup 2. Basically, since the APs antennas are omnidirectional, they don't have back-lobe nulls that can reduce the radiation and limit the Pr level.

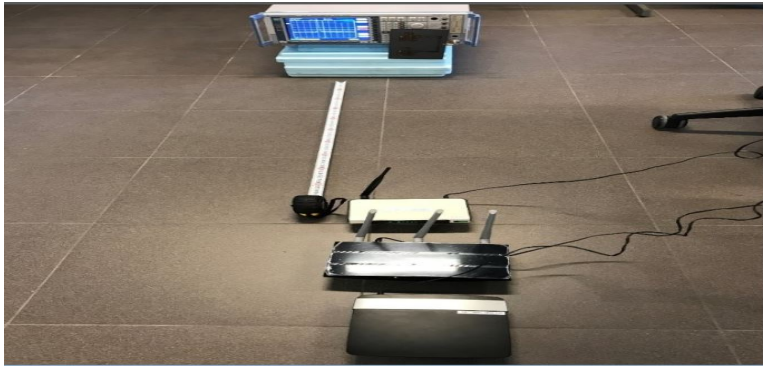


Figure 4.11: Experimental Setup 3: Monitoring the Pr level from 3 APs placed behind each other.

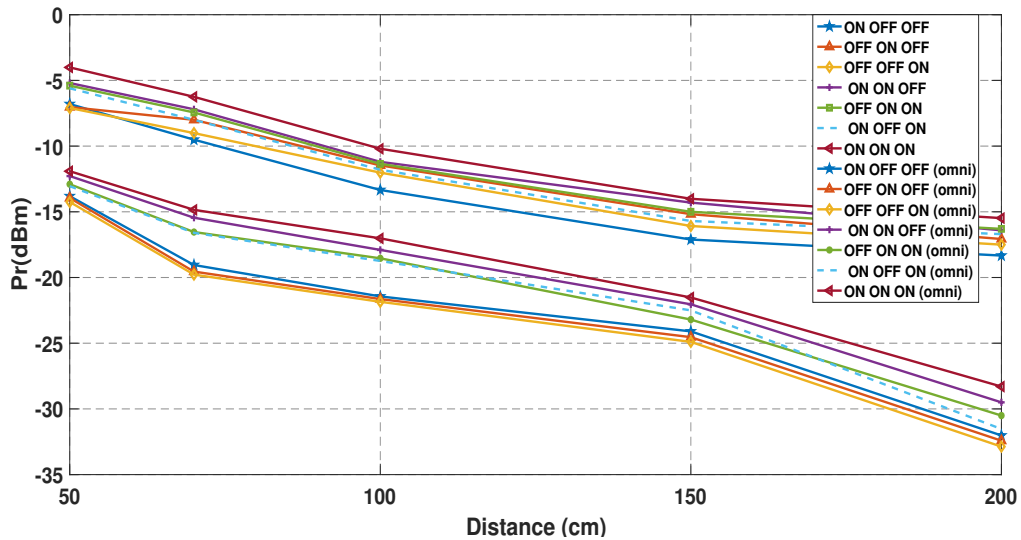


Figure 4.12: Results of setup 3: Pr on meander vs. omnidirectional antenna from 3 APs behind each other.

4.1.4 Comparative Analysis Between Setups

It is shown in Fig. 4.13 that when the APs are behind each other, the Pr level is higher especially in the meander line case. We can see an improvement in the Pr level received from -6.8dBm to -4.01dBm . The reason is that having these routers behind each other enhances the Pt level resulting in a higher Pr level. Even for the same setup, the omnidirectional antenna gives also an improved Pr level from -13.81dBm to -11.91dBm , compared to the the other setups.

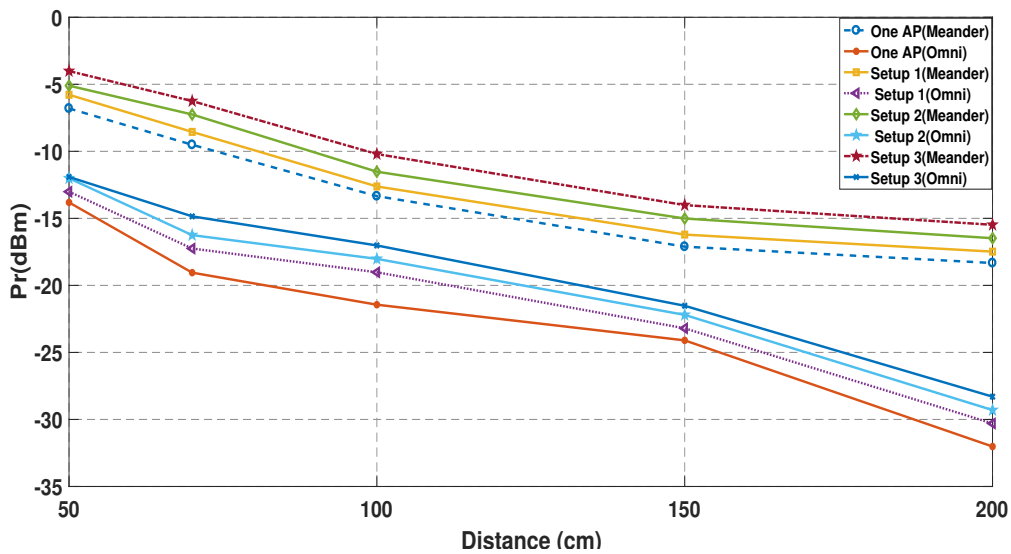


Figure 4.13: Comparing the Pr level when using 1 AP and 3 APs.

Chapter 5

Power Management Circuit

5.1 Existing RF Based Wake-Up Circuit With Active Components

We can find in the literature extensive work conducted on waking up a microcontroller or a sensor from sleep mode using active components such as operational amplifiers. For example, Fig. 5.1 shows an LTC1540 which is an operational amplifier used in its comparator mode [49]. The latter is used by the authors in [50] and is integrated with a designed rectenna system. The LTC1540 has a low current consumption and a built-in voltage reference of 1.13 V. The minimum threshold to turn on the comparator is set to 50 mV through voltage division. Choosing $R1 = 1 \text{ M}\Omega$ and $R2 = 47 \text{ K}\Omega$ and a $V_{cc} = 3\text{V}$, gives $V_{\text{threshold}} = 50.8 \text{ mV}$. Hence, this is an active based circuit that is used for RF wake-up applications. Fig. 5.2 displays the rectenna along with the active comparator. This work also involves addressing using flip flops.

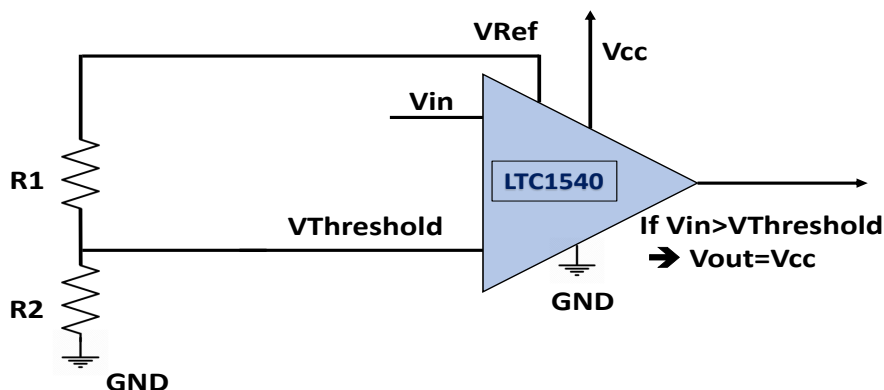


Figure 5.1: LTC1540 circuit diagram.

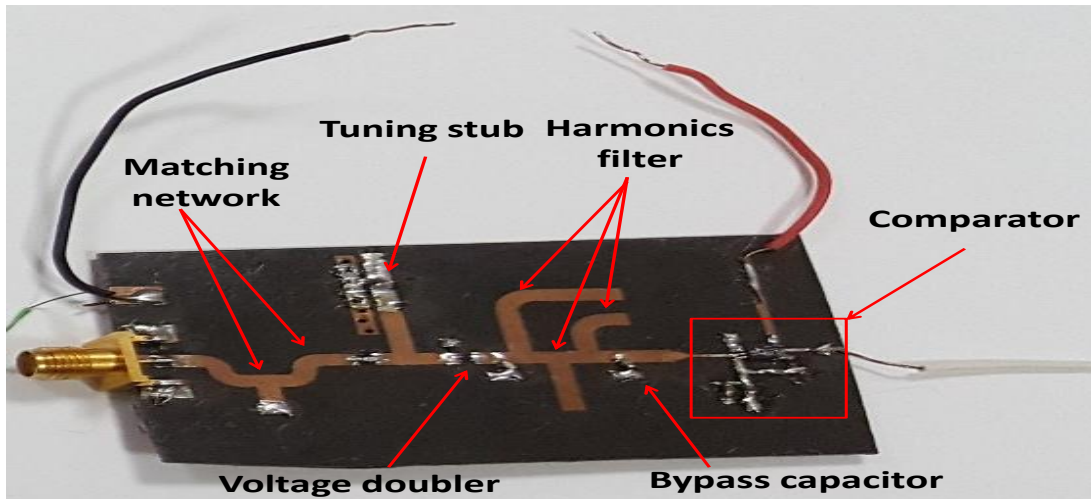


Figure 5.2: Prototype of the wake-up receiver [50].

According to [50], when the wake-up receiver is in active mode, it consumes $13.5\mu\text{W}$; however, if it is in sleep mode it only consumes $4.5\mu\text{W}$. The authors employ the Texas Instrument CC3200 launchpad unit, which includes both a wireless interface and a microcontroller (MSP430) with an embedded antenna. This board has an input voltage range between 1.8 and 3.6V, a $4\mu\text{A}$ current consumption in the hibernate state and around 39.5 mA current consumption in the active mode [51]. Using (5.1), we can conclude that for a continuous active mode operation, the maximum lifetime of the whole system reaches about 2 days. However, the proposed sensor has a standby time that could reach about 14 years.

The authors in [50] also compared the time it takes for a triggered wake-up to take place. In general, IoT applications are characterized by infrequent data transmissions and long sleep cycles. Therefore, the active state only occurs occasionally and for a short duration. Triggered wake-up solutions are therefore better suited to IoT applications than scheduled wake-up solutions. In triggered solutions, the IoT sensors are in the sleeping state for most of the time. As soon as a wake-up signal is detected, the sensors transit to the connected state. This mechanism reduces the energy consumption of the IoT sensor by eliminating the energy waste through idle listening and overhearing. To evaluate the performance of the proposed triggered wake-up IoT sensor in terms of power consumption and life time, the authors compare it with the standard scheduled wake-up sensor that employs the duty cycling technique. The percentage of active per total lifetime (DON) of the triggered IoT sensor is less than that of the scheduled wake-up sensor due to the fact that the triggered wake-up sensor only wakes on demand. Basically, the scheduled sensor wakes up periodically regardless of the need to wake up. Accordingly, several values of the sleep cycle corresponding to

different types of IoT applications are measured with T_{trigger} of 2, 1, 0.5 hours. For example, if an IoT device wakes up for 1 min every 2 hrs i.e., it remains awake 0.83 % of the time [50]. Therefore, if the device was triggered for 0.83% of the time, it will remain operational for 213 days. The life time is calculated using (5.1). In (5.1), the equation includes a multiplication factor of 0.7 which accounts for the external factors that affect the estimated time. The total current consumption is calculated using (5.2).

$$\text{EstimatedTime} = \frac{\text{BatteryCapacity}(mAh)}{\text{DeviceConsumption}(mA)} \times 0.7 \quad (5.1)$$

$$I_{\text{Total}} = D_{\text{ON}}I_{\text{ON}} + (1 - D_{\text{ON}})I_{\text{Sleep}} \quad (5.2)$$

We observe that for the case of scheduled wake-up and triggered wake up (3.3%) the scheduled wake-up has a longer lifetime by a day because it doesn't have the WuRx integrated with it. However, for a wake up on demand feature of an IoT application, a longer sensor lifetime is estimated. For this rectenna system, the maximum wake-up distance that can be achieved is measured. The P_t level is changed using the DD-WRT software and by relying on the packet injection algorithm. Accordingly, the maximum wake-up distance is 2.46m which corresponds to a P_r level of -29 dBm.

5.2 RF Wake-Up Circuit Design Enhancements Using Active Components

5.2.1 Ultra-Low Input Current Amplifier Characteristics

In this section, an ultra-low input current amplifier is used by relying on its comparator mode. Because of the ultra-low input current noise of 0.13 fA/Hz, the LMC6001 can provide nearly noiseless amplification of high resistance signal sources [52]. Furthermore, the LMC6001 operates at input currents as lows as 25 fA. It is suited for applications requiring ultra-low input leakage like sensor amplifiers sensitive photodetection and transimpedance amplifiers. Since the input noise is only 22 nV/Hz, the LMC6001 can achieve a higher signal to noise ratio than any JFET input type electrometer amplifiers [52]. Applications of the LMC6001 include long interval integrators, ultra-high input impedance instrumentation amplifiers, and sensitive electrical-field measurement circuits [52]. Therefore, the LMC6001 is integrated with the rectenna system and is used in its comparator mode. For clarity purposes, this setup is denoted as in lab design 1. Since it is an active component, then a voltage supply, V_{cc} is needed. The LMC6001, compares the output voltage of the rectifier which corresponds to the

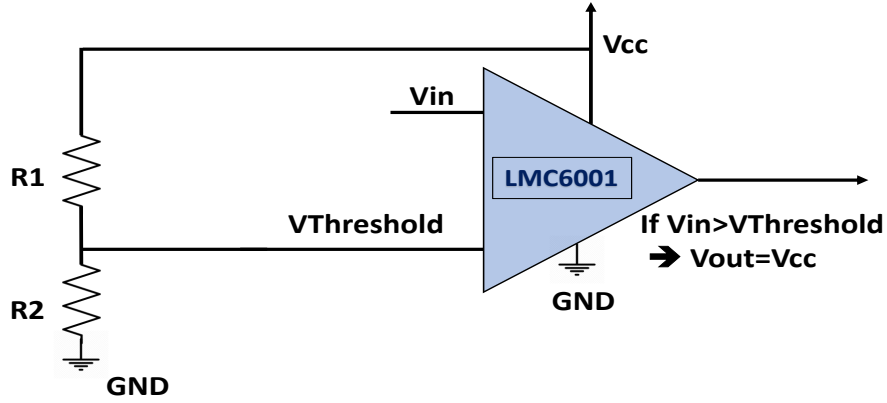


Figure 5.3: LMC6001 circuit diagram.

input voltage of the comparator, with a threshold voltage. This threshold voltage is achieved through voltage division as shown in Fig. 5.3. To have successful wake-up at large distances, the voltage threshold value is chosen to be very small. However, this value can't exceed 0.85mV because this is the inferred voltage noise level. If the threshold voltage was less than 0.85mV , false wake-up will result because the system will wake-up from any noisy signal and not from the triggered wake-up signal. Fundamentally, if the input voltage of the comparator is higher than the threshold voltage, the output voltage will be equal to V_{cc} . The designed system is simulated first on Proteus and then tested in the lab.

To satisfy the constraint that facilitates RF based wake-up at larger distances, the resistors are chosen such that the voltage division gives us a 2mV threshold which is greater than the voltage noise level. For an input voltage higher than 2mV , the comparator switches on and gives an output voltage of almost 3V . In this setup $R1 = 2.2\text{M}\Omega$ and $R2 = 1.51\text{k}\Omega$ as shown in Fig. 5.4.

In the sleep state, the current dissipated is $1.2\mu\text{A}$ and the power dissipated is $3.6\mu\text{W}$. Choosing these particular resistor values, ensures a very low current and thus a lower dissipated power. In the active state, the current is almost $1.36\mu\text{A}$ which is also a very small current value. The current consumed in the active state is that small because the LMC6001 has an internal resistance above $1\text{T}\Omega$ and consumes current in fA that is considered negligible.

Furthermore, if we increased the voltage threshold to higher values, the current dissipated level will decrease. For example, notice that if we increased the $V_{\text{Threshold}}$ to almost 100mV , the current dissipated will decrease to $1.32\mu\text{A}$ as shown in Fig. 5.5. Also, the power dissipated will decrease from $4.08\mu\text{W}$ to $3.96\mu\text{W}$ which is not significant. Therefore, we choose a threshold that guarantees higher wake-up distances.

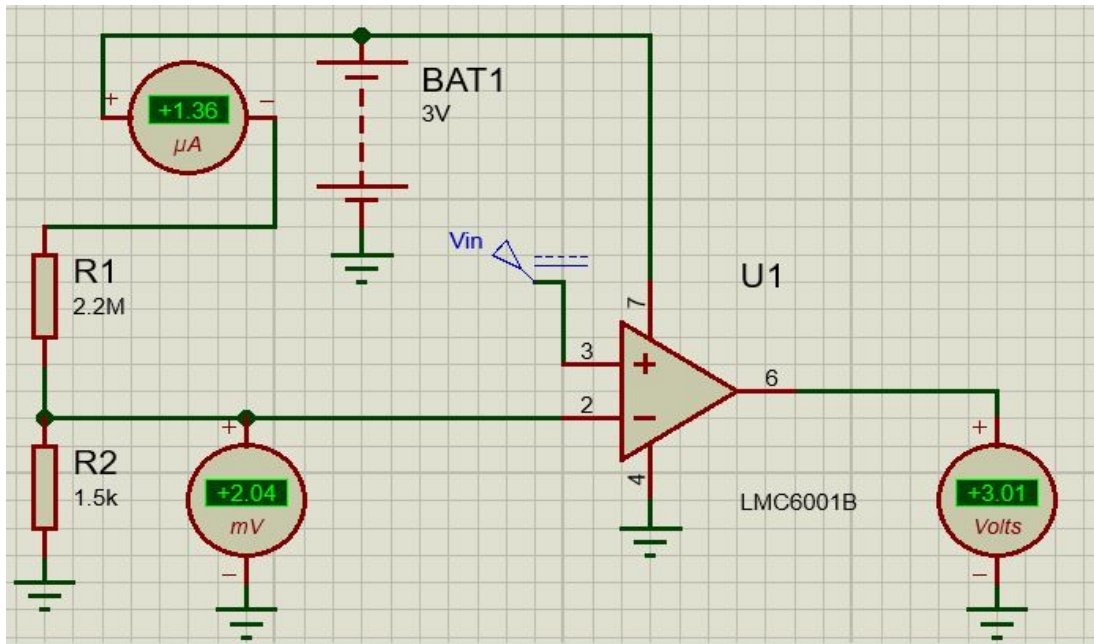


Figure 5.4: The LMC6001 in its comparator mode at 2mV threshold voltage simulated on Proteus.

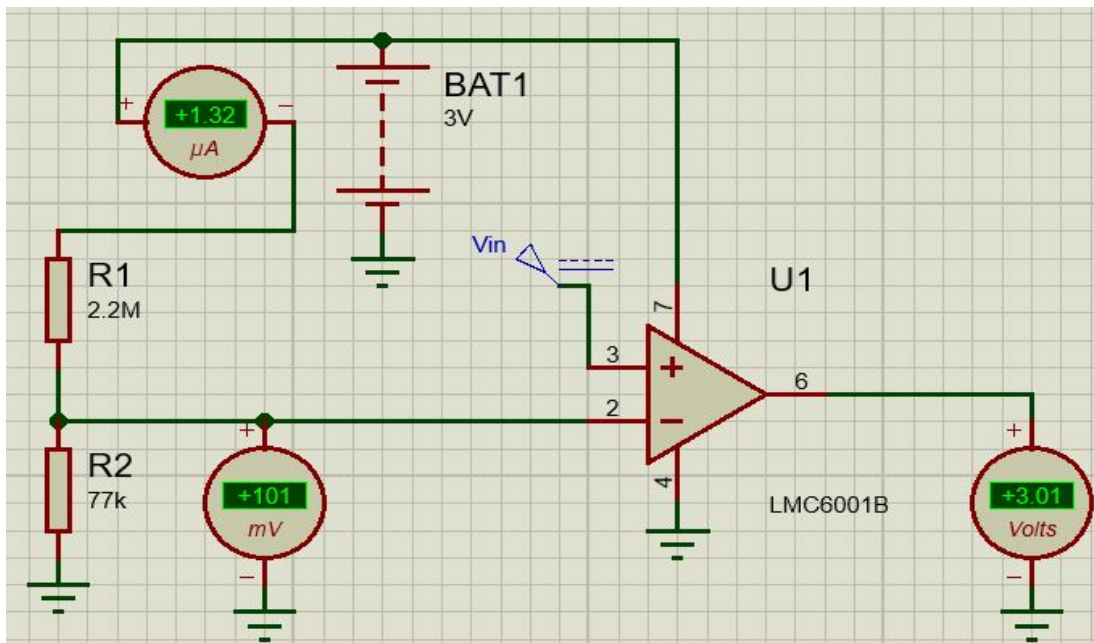


Figure 5.5: The LMC6001 in its comparator mode at 100mV threshold voltage simulated on Proteus.

Additionally, if a device with a longer lifetime is needed, a higher threshold voltage must be chosen. However, in the proposed system, a circuit that serves the application at hand is designed and the appropriate voltage threshold that optimizes its wake-up ability at large distances in a low interference medium is selected. Therefore, in order to quantify the maximum wake-up distance, the LMC6001 is integrated with the rectenna system. For this setup, we are able to wake-up an IoT device at a distance of 5.2m as shown in Fig. 5.6. The voltage at the output and the maximum distance for the active mode are shown in Fig. 5.7. Fig. 5.8 shows that the current consumed when the wake-up circuit is awake is almost $1.36\mu\text{A}$.



Figure 5.6: In lab measured distance for the designed wake-up circuit.



Figure 5.7: Measured distance and output voltage of the wake-up circuit design.



Figure 5.8: Current consumed by the active wake-up circuit.

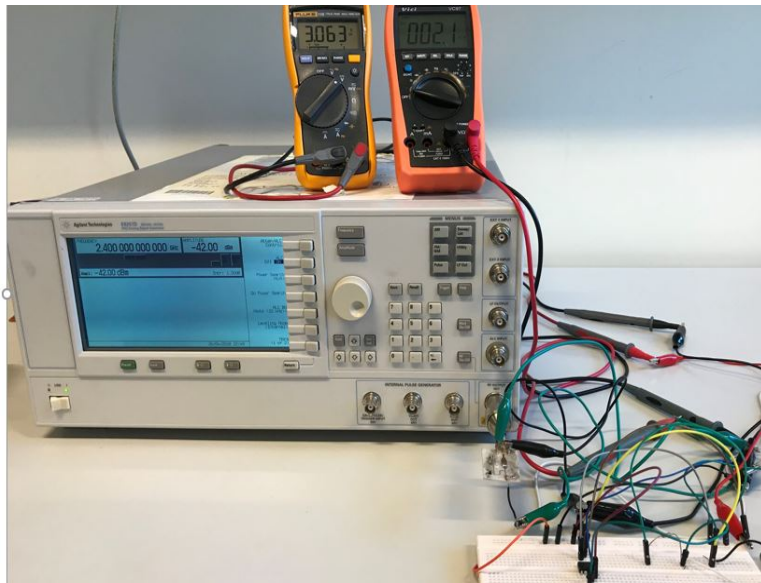


Figure 5.9: Measured power received level of the wake-up circuit design by the signal generator.

After identifying the maximum distance, the P_r level must be identified. Therefore, a signal generator is utilized and connected to the rectifier. Then, the P_r level on the signal generator is decreased until the threshold voltage is obtained. Fig. 5.9 shows the at a P_r level of -42dbm , the threshold voltage is 2.1mV and the circuit works and gives an output voltage of 3V . These ex-

periments were done in the lab and are also subject to interference from indoor routers. Moreover, in order to make sure that the rectenna system with the LMC6001 is waking up from the packet injection algorithm and not from the available signals in the room, the latter system is tested in an anechoic chamber. The chamber absorbs any reflections and external noise from surrounding electromagnetic signals. Therefore, we place the router inside the chamber as shown in Fig. 5.10. The only signals inside the chamber are guaranteed to be from that AP only. Since the chamber's length is smaller than the maximum achieved distance, we decrease the transmit power level from 17dBm to 12dBm. Accordingly, the system only wakes-up when it receives the continuous transmission from the packet injection algorithm. It doesn't wake-up from any external noise source. This proposed system is noise sensitive, so it is practical to wake-up sensors or microcontrollers in a low interference media i.e large green field. For the case of waking up indoor sensors, the threshold voltage must be increased to prevent false wake-up. Hence, for any application, it is crucial to study the environment and detect the interference level and design a system that is both energy efficient and wakes up only when triggered.

Furthermore, since our main objective here is RF wake-up, we connect our design to a microcontroller and we demonstrate the design's capability to wake it up. The microcontroller used is the CC3200 also and we get the corresponding current and power consumption values, in both active and sleep modes in Table. 5.1.

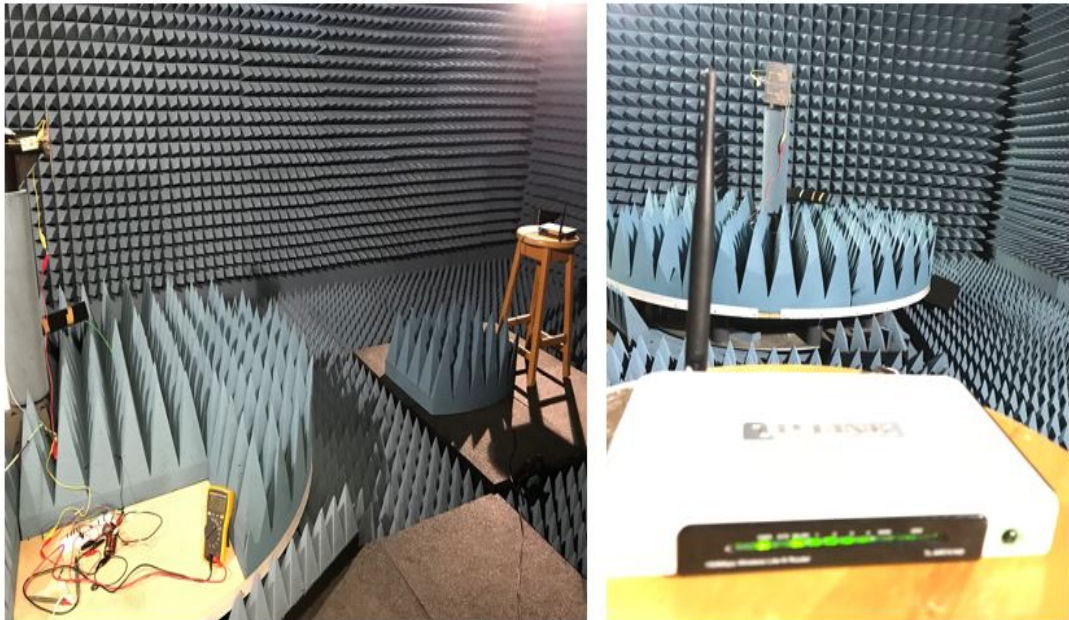


Figure 5.10: Rectenna and the LMC6001 anechoic chamber testing.

	Active (μA)	Sleep (μA)	Active (μW)	Sleep (μW)
Wake-up Rx	1.36	1.2	4.08	3.6
Microcontroller	39500	4	118500	12

Table 5.1: Measured current(μA) and power(μW) consumption for design 1.

5.3 RF Wake-Up Circuit Comparison Between Existing and Enhanced Designs

We can observe important circuit enhancements in design 1 compared to [50]. The circuit is more energy efficient because it dissipates only $4.08\mu\text{W}$ while the circuit in [50] dissipates $13.5\mu\text{W}$ in the active state. Furthermore, we can wake-up devices at larger distances now and maintain an energy efficient system. For a detailed comparison between the two active circuits, we calculate the theoretical life time of each circuit for both scheduled and triggered wake-up using (5.2) and (5.1). The calculated life time disregards electronic circuit degradation or battery age malfunction problems. The values are theoretical and are used to present additional lifetime enhancements between design 1 and the design presented in [50].

Basically, we evaluate the life time of the wake-up receiver and the microcontroller for both designs. Table. 5.2 represent a detailed analysis for the life time for each design. We can notice that the main difference between the triggered and the scheduled schemes is the on-demand characteristic of the triggered wake-up solution. Therefore, the sensor that employs triggered wake-up will be active less frequently. Recall that The percentage of active per total lifetime is denoted by DON. We can notice that the lifetime between the system in [50] and this work is almost the same, but we can spot the differences at lower triggered DON percentages i.e waking up a sensor less frequently. Notice that the difference be-

	[50]	This work
Always on	2 days	2 days
Scheduled (DON= 3.3%)	56 days	56 days
Triggered (DON= 3.3%)	55 days	55 days
Triggered (DON= 1.67%)	114 days	114 days
Triggered (DON= 0.83%)	217 days	218 days

Table 5.2: Evaluating the life time of design [50] and design 1 with respect to the wake-up receiver and microcontroller’s current only.

	[50]	This work
Power Dissipated(μ W)	13.5	4.08
Pr (dBm)	-29	-42
Pt (dBm)	17	17
Dmax (m)	2.46	5.20
Vthreshold (mV)	50.8	2.04
Iout (mA)	10	18
Cost (\$)	3.06	12.24

Table 5.3: Evaluating [50] and this work with respect to different parameters.

tween design [50] and design 1 is highlighted in Table. 5.3. As a result, we can conclude that using design 1 at a Vthreshold of 2.04mV will result not only in a more energy efficient circuit but also in a larger wake-up distance.

5.4 RF Charging Circuit Design Using Passive Components

5.4.1 DC-DC Power Converter Characteristics

In this section, we will introduce a complete passive system that relies on a boost converter. For clarity purposes, we will refer to this setup as design 2. Basically, in this design a step up DC–DC power converter is utilized to increase the voltage at the output of the rectifier in order to charge the battery of a microcontroller or an IoT device. Basically, the DC–DC step up converter is a class of switched-mode power supply (SMPS) that contains a diode and a transistor and an energy storage element. Therefore, integrating the DC–DC boost with the rectenna system guarantees a complete passive system utilized in RF charging applications. Therefore, in order to create a complete passive system, it is crucial that the DC–DC boost converter doesnt have any biasing circuitry i.e a voltage source.

Therefore, the LTC3108 which is a highly integrated DC–DC converter is chosen among others because it is ideal for harvesting and handling excess energy from extremely low input voltage sources such as thermoelectric generators thermopiles and small solar cells. Typical applications where the LTC3108 is used are: remote sensors and radio power, HVAC systems, wireless sensing, automatic metering, and others [53].The step-up topology operates from input voltages as low as 20mV. The LTC3108 utilizes a small step-up transformer to boost its voltage. The typical transformers used have a 1:20, 1:50 and 1:100 primary to secondary ratio. As the number of turns in the secondary transformer increase, we can start boosting from lower input voltages and have a fully operating system.

VS1	VS2	Vout
Gnd	Gnd	2.35V
Vaux	Gnd	3.30V
Gnd	Vaux	4.10V
Vaux	Vaux	5.00V

Table 5.4: VS1 and VS2 different configurations that can change the voltage at the output of the DC-DC boost.

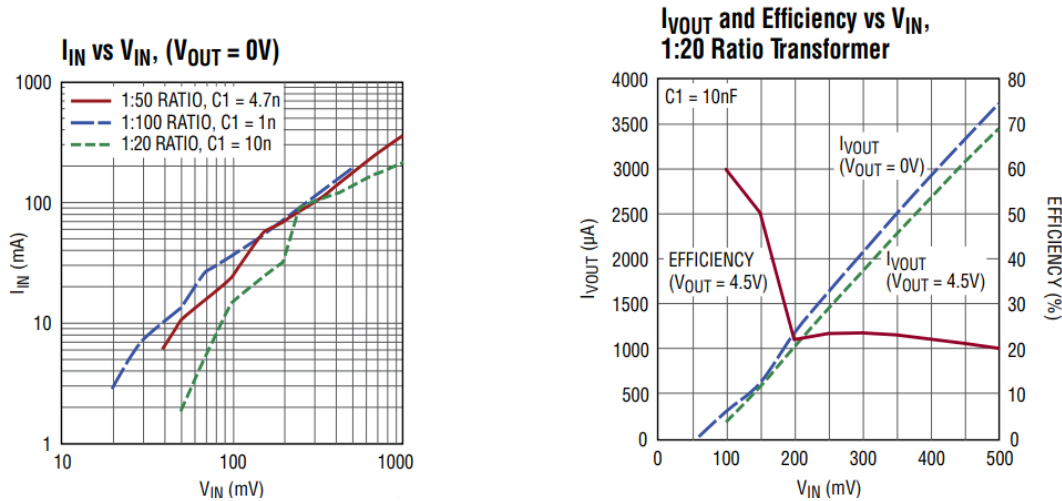


Figure 5.11: LTC3108 input current and voltage behavior for different transformer windings [53].

For example, a 1:20 transformer could start boosting from an input of 60mV, while a 1:50 starts at almost 40mV, and the 1:100 transformer starts boosting from a voltage of nearly 20mV. However, if we choose the 1:100 ratio transformer the current will get divided by 100. This is critical because it decreases the power needed for the boost to operate.

It is important to connect both pins, VS1 and VS2 properly because they determine which value we need at the output. Table. 5.4 shows the different configurations to get the desired output voltage. For our designed boost, the VS1 and VS2 are connected to Vaux resulting in a 5V at the output.

According to Fig. 5.11, if we use a 1:20 transformer, the DC–DC boost operates at an input voltage of 50-60mV at an input current of 2mA. As the number of turns in the secondary transformer increases, the current needed for the boost to operate will also increase. Moreover, we can notice that using a 1:20 ratio transformer is more efficient at higher input voltages. In our prototype design, a 1:20 transformer from Wurth Electronik is used. The transformer has a 6.4x6.4mm dimensions [54]. The boost system requires a C1=10nF, C2=330pF, C3=1μF and C4=10μF to operate as shown in Fig. 5.12. The capacitors' dimensions range between 1x1mm to 1.5x1.5mm.

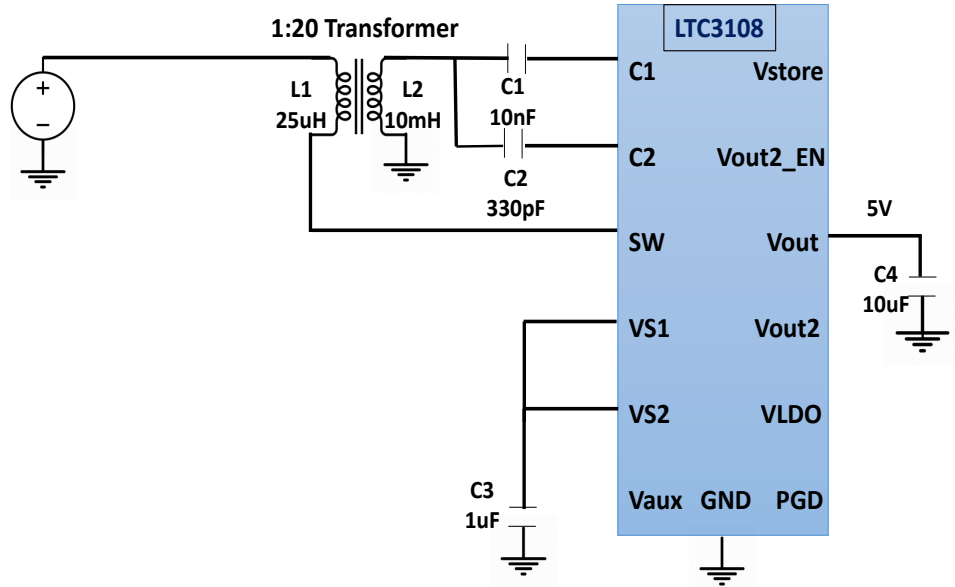


Figure 5.12: DC-DC boost composed of a 1:20 transformer, $C1=10\text{nF}$, $C2=330\text{pF}$, $C3=1\mu\text{F}$, and $C4=10\mu\text{F}$.

5.4.2 Performance of Designed Passive System

After choosing the 1:20 transformer and the proper capacitors for the circuit, the LTC3108 is fabricated as shown in Fig. 5.13. To test the functionality of the fabricated design, we connect the boost to the power supply. Fig. 5.14 shows that at an input voltage of 64mV , the fabricated boost give an output voltage of 4.99V .

Now that we have all the specs of the DC-DC boost, the latter will be integrated with the rectenna to create a complete passive system. First, we connect the rectifier to a dedicated signal generator to determine the minimum received power that is required to have a functional system. The measured P_r is calculated to be almost 7dBm which is considered higher than the P_r level we had in earlier sections. Recall that in the previous sections, for a P_t of 17dBm , the P_r level was -6dBm at 50cm . The V_{out} was almost 0.4V at a $1\text{k}\Omega$. However, when we connect the DC-DC boost with the rectifier using the previous setup, the voltage at the input of the boost dropped to 5mV . This value is considerably lower than the required input voltage for an operational boost. Basically, the LTC3108 has a corresponding impedance of 40Ω , which leads to this significant drop in the voltage at its input. Therefore, we need to increase the power level received to 7dBm to have a functional system. Since the signal generator could reach a max P_t of 12dBm , we can add a 10dB power amplifier that increases the P_t to 22dBm . Using an RF sensing device at the receiving meandered line antenna, the P_r at 1m

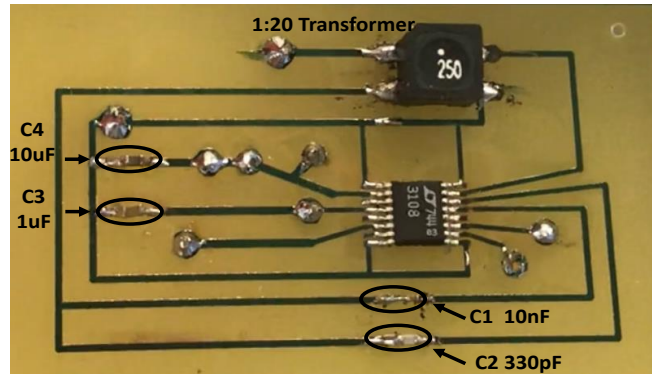


Figure 5.13: Fabricated DC-DC boost.

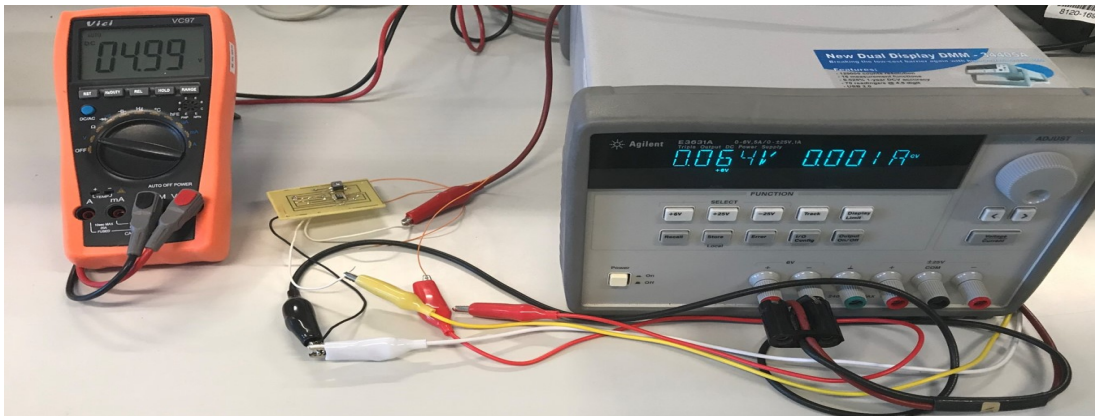


Figure 5.14: Testing the functionality of the fabricated DC-DC boost.

distance is almost 7.07dBm and the boost system operates properly. However, in order to increase the distance further, another power amplifier with a 5 dB gain is introduced at the receiver. The received power is measured to be around 7.62 dBm. Fig. 5.15, displays the positions of the amplifiers and the voltage received at the input of the boost that is almost 80mV. Since this voltage level is greater than the threshold, the resulting output voltage will be 5V. In this case the measured distance is 1.6m. We can achieve a maximum distance of almost 1.8m when the power received level is 7dBm exactly. However, fluctuations may cause the power received level to drop and the voltage level will not be sufficient to activate the DC-DC converter. Accordingly, choosing a slightly higher value is recommended to guarantee the proper functionality of the proposed passive system.

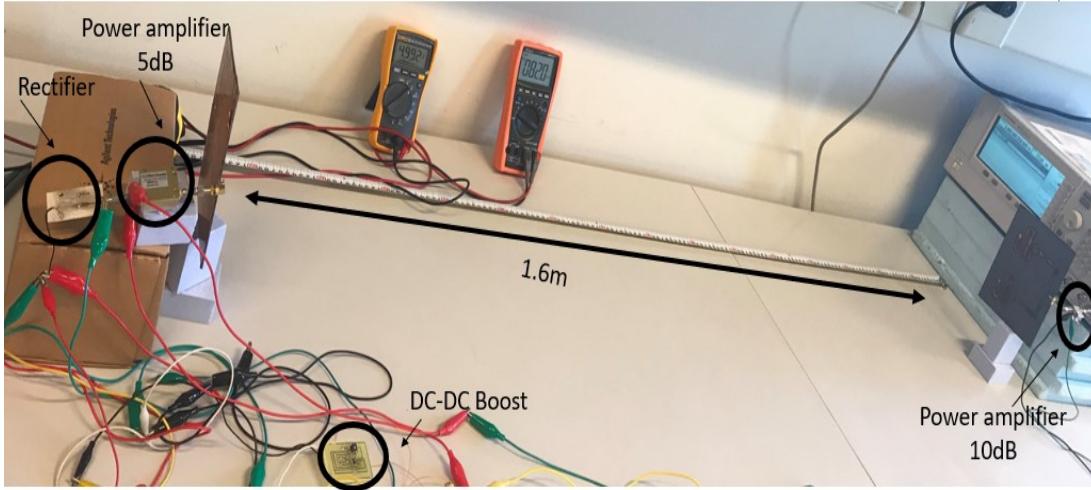


Figure 5.15: Maximum charging distance using the passive system.

Pt (dBm)	Gain Tx (dB)	Gain Rx (dB)	Pr (dBm)	Distance (m)
22	12.56	12.56	7.078	1.0
22	12.56	17.56	7.62	1.6
23	12.56	12.56	7.22	1.1
23	12.56	17.56	7.22	1.8
25	12.56	3.00	7.01	0.5
25	12.56	12.56	7.18	1.4
25	12.56	17.56	7.53	2.3
30	12.56	3.00	7.45	0.8
30	12.56	12.56	7.12	2.5
30	12.56	17.56	7.20	4.4

Table 5.5: Different Tx power, and antenna gains.

$$P_r = \frac{P_t G_t G_r \lambda^2}{(4\pi R)^2} \quad (5.3)$$

Fundamentally, Table. 5.5 shows different possible configurations for the transmit power level with diverse Tx and Rx antenna gains, that will result in a Pr level slightly greater than 7dBm. The values obtained rely on the simplified Friis transmission equation given in (5.3), where P_t represents the transmit power, P_r is the power captured by the antenna, G_t denotes the transmit antenna gain, G_r is the received antenna gain and R is the distance of separation between the transmitter and receiver [55].

5.4.3 Charging a Battery from a Passive Circuit

After identifying the necessary parameters for a functional passive system, it is required to charge a NiCd 2.4V 300mAh battery. Basically, there are four different ways to charge a NiCd battery. We can charge the latter either through a semi constant current charge, or a timer controlled charge, or a differential voltage cutoff charge, or a differential time cutoff charge, or a trickle charge [56]. Each charging method has its own characteristics that range between reliability, temperature tolerability, popularity and economical feasibility. Since we want to charge this battery repeatedly every time its capacity is drained, we choose the trickle charging method. This method is simple, economical and applicable to the equipment for long continuous charging. Trickle charging maintains an almost constant current while keeping the cell temperature and internal cell pressure at a safe level. Therefore, we setup an experiment using the DC-DC boost and connect it in such a way to charge the battery. We start with a completely discharged battery and we monitor the time it takes to reach its full capacity. Fig. 5.16 shows the charging duration. According to [56], the battery reaches almost 70% of its capacity quickly and then it continues steadily to reach its 100% capacity. An internal transistor that acts as a variable resistor in the NiCd battery accommodates to the increase in voltage level since the current remains constant. The current consumed is almost 5.5mA which is 1.8% of the capacity of the battery. Accordingly, the battery took almost 21 hrs to reach its optimum voltage.

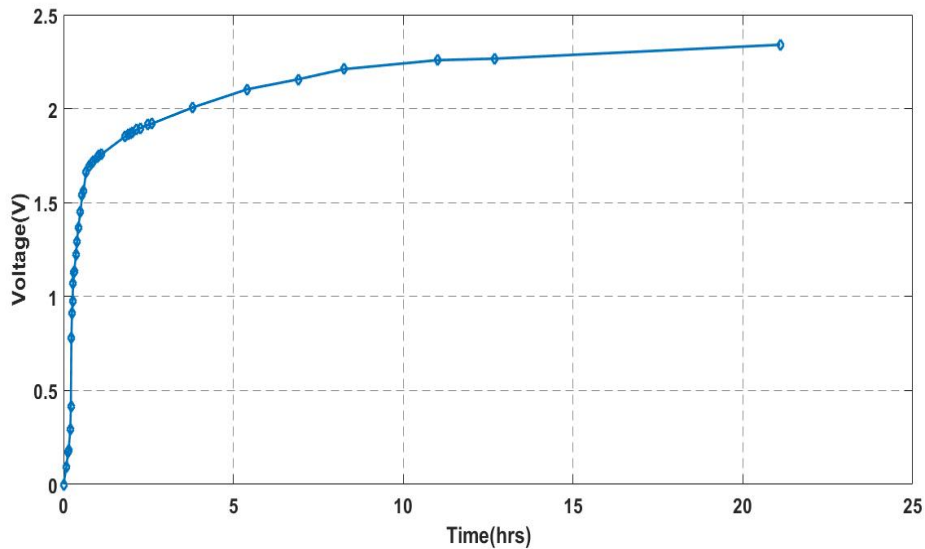


Figure 5.16: Charging duration of a 300mAh NiCd battery.

5.5 Comparative Study Between Active and Passive Setups

In sections 5.1 and 5.2, design 1 and [50] included active components that are used for RF wake-up applications. On the other hand, design 2 is a passive system for RF based charging applications. However, active components can be implemented for charging and passive components can also be proposed for wake-up. Therefore, if we use one of the active designs for charging a battery, it would be like charging a battery directly from a V_{cc} source i.e another battery. The battery that we are trying to charge will automatically reach its maximum capacity within almost two hours because it is draining current from the other battery source as much as possible. For this type of charging, the current is not limited and cannot be controlled. In addition, the V_{cc} battery will drain its capacity quickly which results in an energy inefficient system. Hence, active designs are a better fit for wake-up applications because an active component's battery will deplete faster if it is always activated. Hence, having a passive system for charging is more energy efficient than that of an active design for RF based charging applications. Moreover, we can use a passive system for RF wake-up applications as well. Recall that in design 2, the DC-DC boost system required a high P_r level of 7dBm in order to function properly. Thus, a higher P_r level limits the system's ability to wake-up sensors at large distances. However, using an active circuit such as the one in design 1, a P_r level of -42dBm is enough to wake-up sensors in a wide range. As a summary, Fig. 5.17 shows each design's performance for RF based charging applications or RF based wake-up applications. We observe that charging using active design 1 is not as energy efficient as using active design 2 for wake-up. Mainly if we are charging a device using an active system, the system will be activated for a longer duration hence dissipating additional power than the case where it is intermittently activated. On the other hand, a complete passive system is the most efficient because no voltage source is needed, however a range problem will arise. As a conclusion, it depends on the use case of each design. Many parameters such as location (indoor or outdoor), charging, wake-up, P_t , P_r , antenna gains, frequency of operation, interference, distance, power dissipated and others can greatly affect the performance of each design. Basically, the user must deploy the optimal design for the respective application.

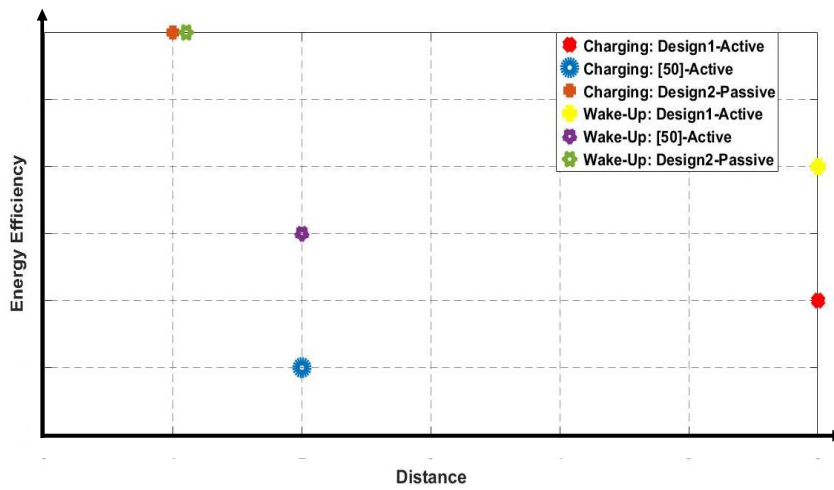


Figure 5.17: Comparing the charging and wake-up capabilities for increasing energy efficiency and distance.

Chapter 6

Case Study: Smart Agriculture

6.1 Indoor Experiment in Lossless Media

The maximum achieved voltage at the output of the rectifier is around 386 mV at a load of 1 K Ω , transmit power of 17 dBm, and a distance of 50 cm. Even though the circuit is able to rectify signals efficiently from the Wi-Fi router, this DC voltage is not sufficient to wake-up typical IoT devices. Therefore, a boost circuit is required to step the rectifier's low output voltage to a higher level. In this section, the rectifier circuit is integrated with a comparator to complete the RF wake-up device.

For this experiment, design 2 of the power management unit is used with the rectenna system. A DHT-22 temperature sensor [57], and a CC3200 unit [51] are used to read and transmit data. The LTC1540 comparator has a low current consumption and a built-in voltage reference of 1.13 V. The minimum threshold to turn on the comparator is set to 50 mV. The CC3200 includes a wireless interface that can be used to connect the sensor to a remote cloud server for data exchange, in addition to an MSP430 microcontroller and an embedded antenna. When the CC3200 receives an interrupt signal from the comparator's output indicating a rectified voltage that exceeds 50 mV, it senses temperature for around 30 sec through the connected DHT-22 sensing element and uploads the sensed data to the cloud server over Wi-Fi.

To measure the DC voltage at the output of the rectifier, the distance between the router and the designed circuit is varied from 50 cm to 300 cm. Fig. 6.1 demonstrates the voltage level variations before reaching the comparator in order to achieve the desired voltage level of 50 mV. Thus, as can be noted in Fig. 6.1, the maximum wake-up distance is around 246 cm at a transmit power of 17 dBm which corresponds to a sensitivity of -29 dBm. The output voltage after the comparator stage is 2.7 V which is sufficient to power the CC3200 and switch it from sleep to active state. Through this technique, the designed temperature sensor wakes-up and senses data at ranges up to 2.46 m only if the router is transmitting and while the packet injection algorithm is applied.

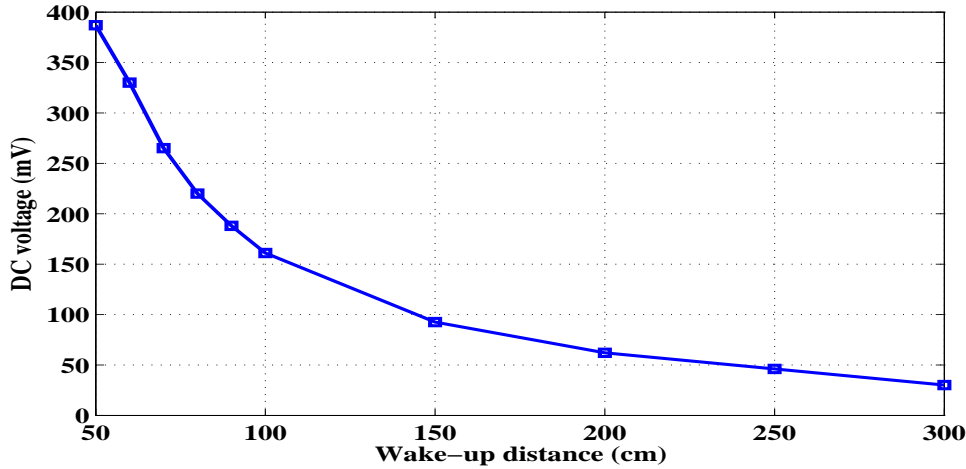


Figure 6.1: DC voltage as function of the wake-up distance of the indoor experiment.

6.2 Outdoor Experiment in Lossy Underground Media

With the recent advancements in communication techniques, WSNs have enabled a variety of novel applications. Among these applications, Wireless Underground Sensor Networks (WUSNs) are attracting attention and constitute a promising area with great potential that will enable a wide variety of new applications that were not feasible with earlier technology [58]. WUSNs mainly focus on the use of wireless sensors that are only buried a few meters deep in the soil or sand. Moreover, WUSNs have many notable merits when compared to wired underground sensor networks. These merits range between concealment, timeliness of data, reliability, easy deployment and coverage density [59, 60]. Therefore, WUSNs will play a major role in potential applications for smart agriculture, infrastructure monitoring, sport’s field maintenance and others [58]. It usually targets irrigation and environmental monitoring application and provides a wireless communication capability that was absent earlier. The data is processed in real time which gives us accurate and precise results. However, the main challenge that accompanies WUSNs is the propagation medium. Mainly the electromagnetic wave propagation properties in soil is very different than that in air [61]. To this end, the underground wireless channel will be completely distinct from the terrestrial wireless channel. Therefore, establishing an appropriate channel model is essential to make WUSNs feasible.

Current work exists to characterize such an underground communication channel. Soil moisture content, soil homogeneity, soil composition and temperature are the main parameters that impact underground channel modeling [62].

These aspects directly affect the connectivity and delay successful communication. For WUSNs, the environment along with the burial depth and the frequency of the electromagnetic wave impact the communication channel.

Since sand is a dielectric material, the electromagnetic wave propagation is directly related to the sand's dielectric constant. Basically, smaller dielectric constants lead to better wave propagation conditions. However, the presence of water in sand makes communication harder. The quantity of water in sand also contributes to the electromagnetic wave attenuation [63]. This quantity is referred to as volumetric water content (VWC). Mainly, the dielectric constant varies with this VWC parameter. Besides the VWC, the dielectric constant of sand is a non-linear function of frequency [58]. Frequencies around 1GHz present an acceptable and reasonable dielectric constant and as the frequency decreases to 300MHz, the attenuation gets smaller. However, for smaller frequency values, the wavelength will increase, which will result in a bigger sized antenna. Therefore, researchers limit their experiments and testing for WUSNs with frequencies above 300MHz. According to [64], efficient communication between sensor nodes above or buried underground is possible at a distance of 50cm at 2.4GHz. In [58], they present a two-path channel model that characterizes the path loss model while varying both the operating frequency and VWC. The fluctuation is a result of the constructive and destructive interference of the second path. As the frequency and the VWC increase the path loss will also increase. In order to quantify the VWC in sand, researchers in [61] have used a time domain reflectometry (TDR) that monitors the rapid changes in the water content. Accordingly, they measured the dielectric constant of different types of sand as a function of VWC. After identifying all the main parameters that affect underground propagation, the main focus now is on measuring the efficiency of the rectenna system with the packet injection algorithm in an underground setup. For this experiment, we chose fine sand and accordingly conducted some measurements when the rectenna system is buried under sand.

6.3 Experimental Setup

The underground experiments were conducted on AUB campus, specifically in the engineering department. The main objective of the underground experiments, is to find the appropriate depth to place the rectenna-sensor system and still be able to efficiently wake-up and charge this sensor. A comparative study between two different setups is conducted. For the first setup, the rectenna system is buried under dry sand but for the second setup, the rectenna is buried under slightly wet sand as illustrated in Fig. 6.2. For each setup, the voltage of the rectenna system is measured at different depths.

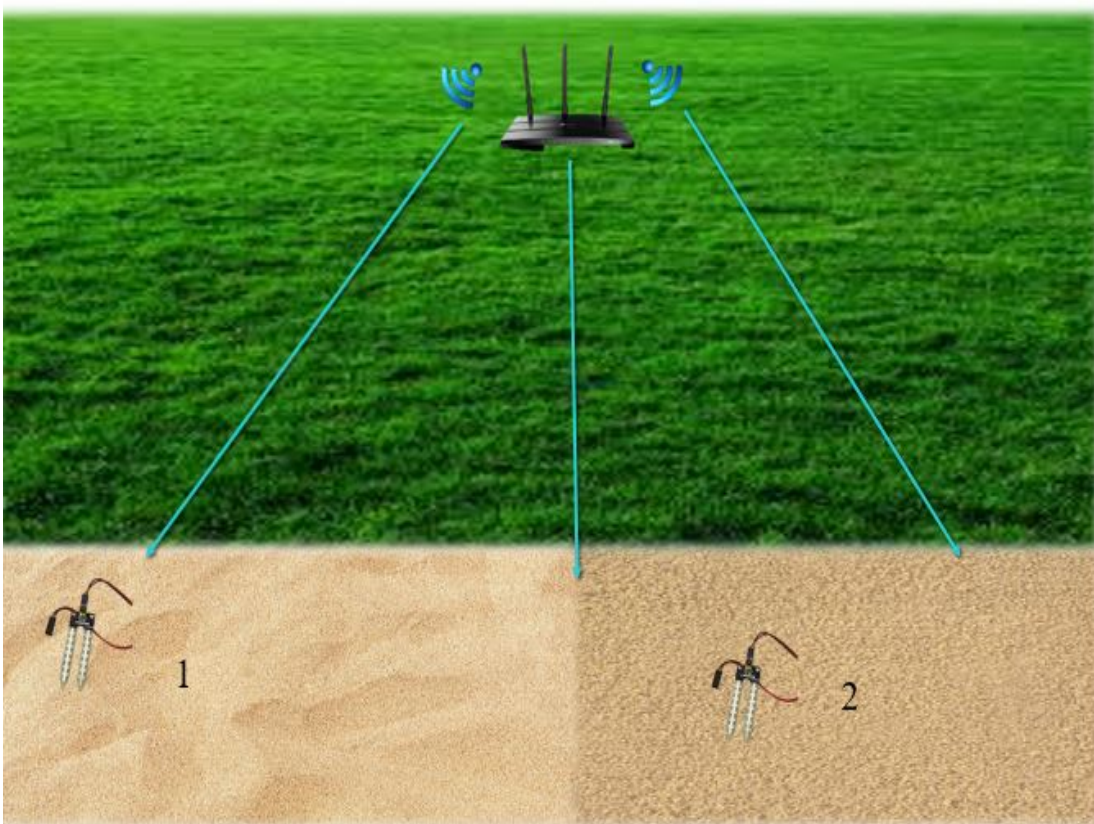


Figure 6.2: Experimental setup of sensors buried in dry sand and slightly wet sand.

6.3.1 Fine Sand and WUSN

Since we are using fine sand, the dielectric material is almost 2.5 when the VWC is 0 [61]. Moreover, we also use a thin plastic pipe and label it at different depths to keep track of the the different altitude levels. For this experiment, an omnidirectional 3dBi antenna is connected to the rectifier and using a voltmeter, we measure the voltages at each depth. The packaging of the rectenna system is shown in Fig. 6.3. The rectenna system is wrapped by a foam material that has a dielectric constant of 1. Basically, a router running the designed algorithm transmits packets at a power level of 17dBm. Fig. 6.4 shows that the distance from the Wi-Fi router to the pipe is almost 50cm.

The pipe is 50cm long with a 50cm diameter. It is labeled from 10cm to 50cm as shown in Fig. 6.5. At every level, we lower the rectenna system and cover it with fine sand and measure the value of the voltage. The pipe used in this experiment introduces additional reflections and can also lead to some losses as



Figure 6.3: Rectenna packaging.



Figure 6.4: Distance from the router to the pipe.

well. In order to quantify the measured losses, the rectenna system was placed inside the pipe when its empty. The voltage is measured also outside the pipe. Accordingly, the pipe introduces almost 10-20mV loss in the received signal. Next we start varying the rectenna system for the case of dry sand. Ultimately, we can recall that in the dry sand case, the dielectric constant is 2.5 [61]. For the second setup, we add distilled water to the sand uniformly and we evaluate the voltage received when the rectenna system is buried under the slightly wet sand.

The volume of the plastic pipe is almost 0.098m^3 that corresponds to 98liters. To ensure a uniform sand-water composition, we use a 1.57L bucket and we filled it with 20% water and 80% sand which is 0.314L and 1.26L, respectively. As a result, the voltage level drops even more when the rectenna is buried under the wet sand. Fig. 6.7 shows the variation in the voltage level for each setup at different depths .

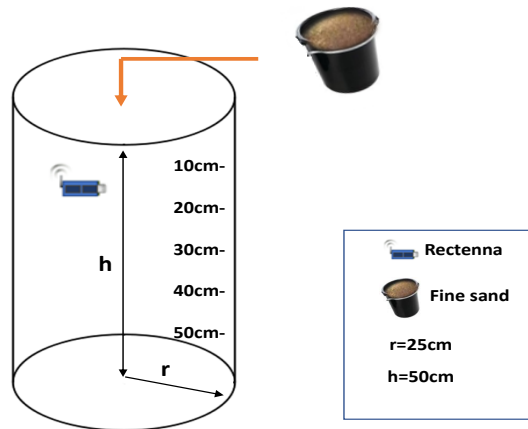


Figure 6.5: voltage is measured as the rectenna is lowered in the pipe and covered with sand.

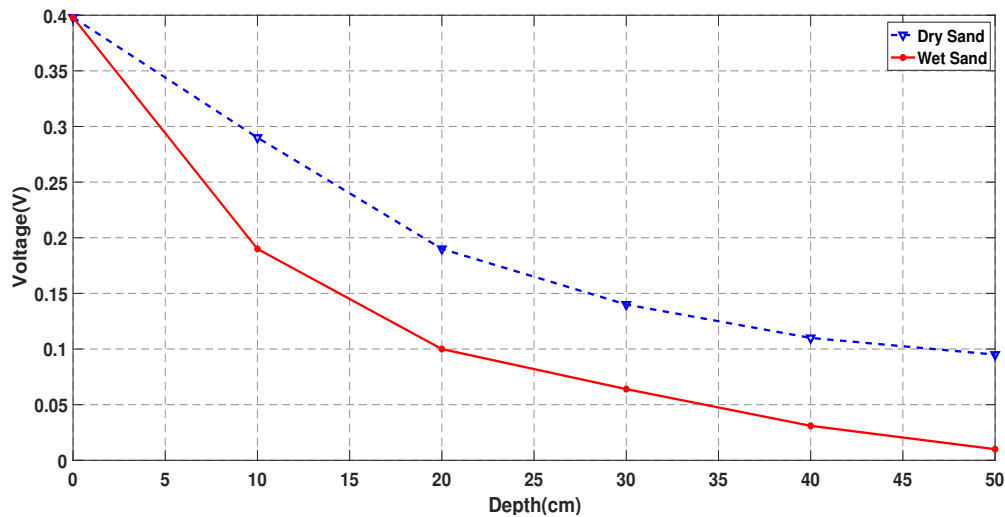


Figure 6.6: Comparing the voltage results of the rectenna when buried either under dry sand or under slightly wet sand.

6.4 Remote Sensing Using A Drone

After verifying that underground communication in a lossy medium is feasible, basic means of Wi-Fi signal transmissions are examined. Hence, we will study the ability of harvesting Wi-Fi signals from a dedicated continuous Wi-Fi signal mounted on a drone.

The main contribution so far validates the effectiveness of our proposed algorithm in indoor environments and outdoor WSNs. For outdoor scenarios such as smart agriculture, the field is filled with soil moisture irrigation, temperature sensors and others and are spread out on the field. However, typical distances separating sensors from each other and from the AP range between 5 to 20m. This problem limits harvesting from a fixed AP. Therefore, there is a need to have a mobile transmitter that ensures RF wake-up and RF energy harvesting. Consequently, a drone that flies over the field serves as a promising solution. The basic use of drones in environmental applications focuses on taking pictures of the field. These pictures help specialists to identify many vegetation problems. Therefore, using a drone to wake-up sensors and recharge batteries on top of taking pictures will lead to the birth of smart agriculture. In this section, a drone hovering over the field at different heights will be examined. The voltage received level at the output of the rectenna system is studied in detail to find the optimum approach for either RF wake-up or RF charging applications. The following experiment is conducted in Turin, Italy. It is a collaboration between AUB and CNR-IEIIT.



Figure 6.7: RF energy harvesting from the drone's telemetry signals.

For this experiment, a drone is sending RF telemetry signal at a power transmit level of 20dBm. These telemetry signals operate at the same GPS frequency and herein send the drone's location information. Our aim is to capture these telemetry signals that are sent over 2.4GHz and convert them into voltage in order to wake-up a field sensor. As a result, two different setups are conducted and in each, we measure the proximity and the maximum distance that the drone needs to fly over in order to achieve a successful wake-up.

6.4.1 Drone's Flying Approach 1: Vertical

In the first approach, a patch antenna that operates at 2.4GHz is connected to the rectifier to mimic a sensor node as shown in Fig. 6.8. The rectenna system is placed at 1.8m from the ground level. In the first approach, the drone hovers the field vertically at a height of 15m with respect to the ground level. Then the drone starts to decrease its altitude until it reaches a height of 5m as shown in Fig. 6.9. For the vertical approach, the maximum received voltage was 80mV when the drone scavenges the field at a height of 5m as illustrated in Fig. 6.10. Fig. 6.11, shows the voltage received levels for different drone altitude configurations.

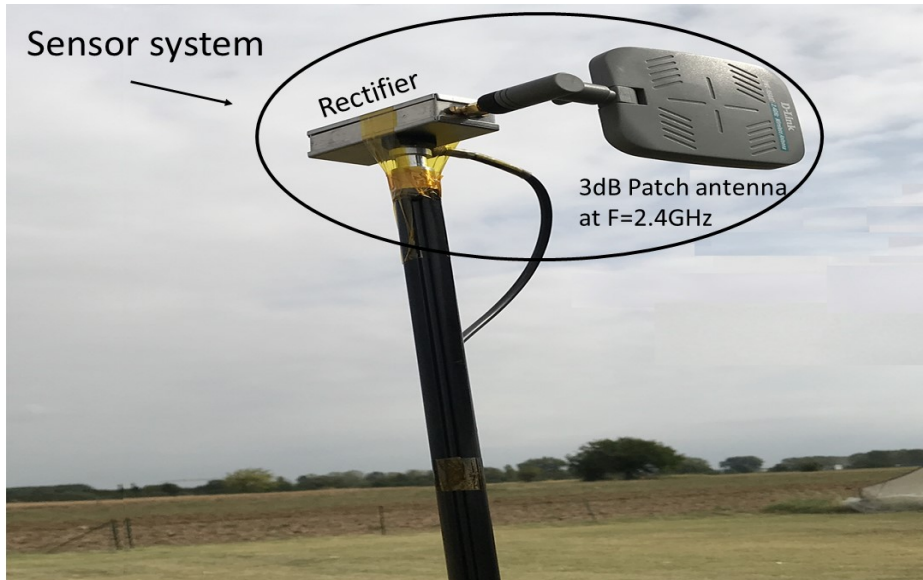


Figure 6.8: Sensor system composed of a rectifier and a 3dB patch antenna.



Figure 6.9: Vertical approach: Drone flying over the field starting at an altitude of 15m and reaching 5m.

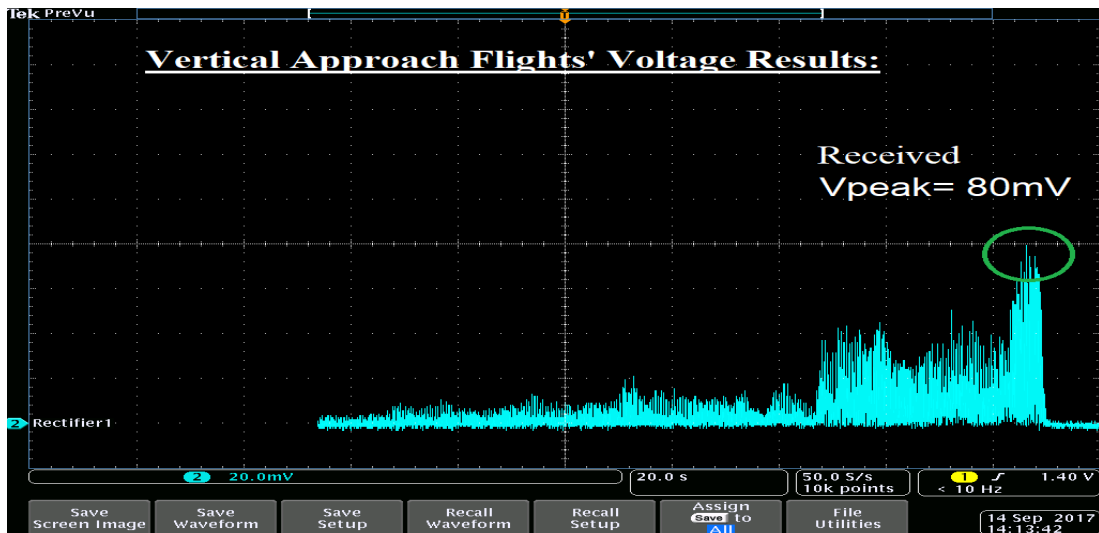


Figure 6.10: Vertical approach: Voltage received.

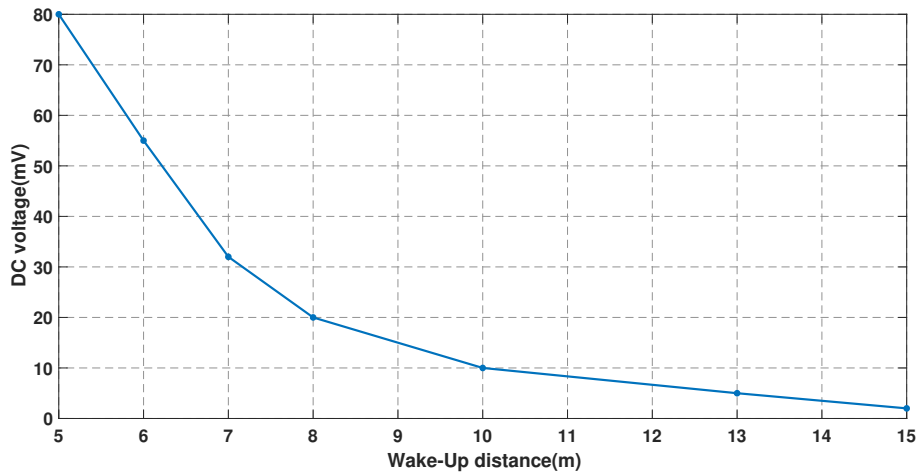


Figure 6.11: Vertical approach: Wake-Up distance.

6.4.2 Drone's Flying Approach 2: Raster

The drone can fly over the field horizontally as well. Therefore, we need to find the optimal approach that can guarantee a triggered wake-up. Thereafter, the same setup as before where the patch antenna and the rectifier system mimic the whole sensor node, is now tested for the case where the drone approaches the field in a horizontal/raster manner. The drone maintains a steady 5m altitude from the ground level. Fig. 6.12 shows that the maximum voltage received level is 20mV.

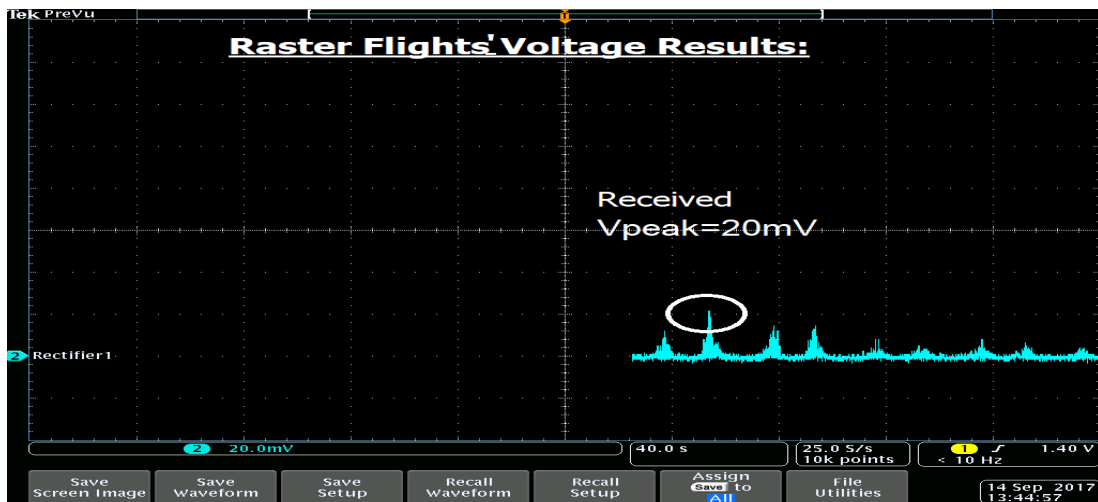


Figure 6.12: Raster approach: Voltage received.

6.4.3 Comparison Between Approach 1 and 2

According to the voltage results, using a drone for RF wake-up is achievable. We can notice that when the drone was hovering vertically, the antenna's power received level was higher than the raster case. Basically, since the drone is maintaining an almost stable position perpendicular to the plane of the sensor node, the antenna's reception level is better. However, in the raster case, the drone was flying from left to right and vice versa over the field which limits the power received at the patch antenna. Hence, the results in Fig. 6.13, present the voltage results. As a result, in both cases we are able to rectify the drone's telemetry signals and we can wake-up sensors. Fundamentally, using the power management circuit designed in section 5.2, the LMC6001 amplifier can successfully wake-up field sensors for both approaches. However, for the vertical approach case, the voltage level is higher since the power received level is higher. Hence, we can use the latter for RF based charging applications as well and not limit its application for RF based wake-up applications. The designed DC-DC boost will function accordingly and charge sensor fields batteries. Mainly, for each application it is crucial to choose the most adequate approach that can achieve both, optimal distances and energy efficiency purposes.

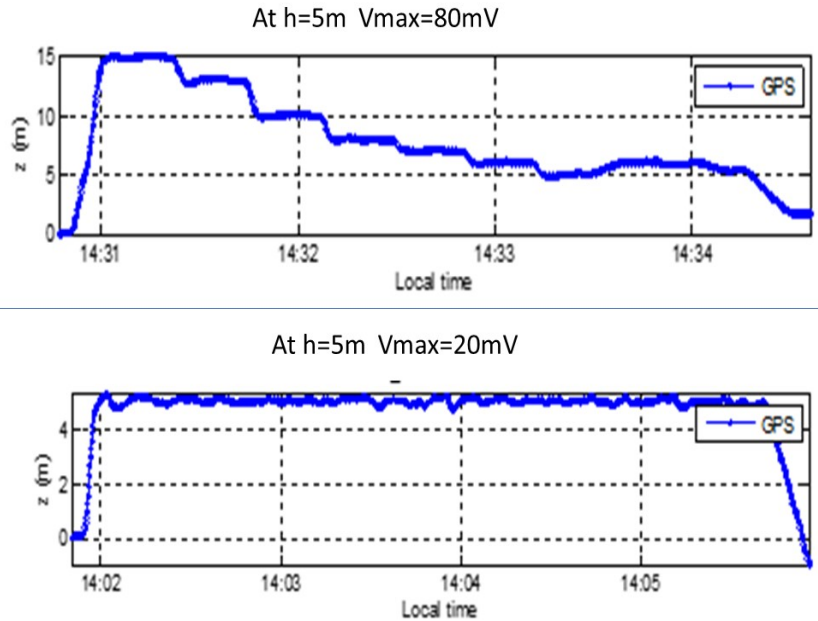


Figure 6.13: Vertical and Raster approach distance variations and maximum achieved voltage.

Chapter 7

Conclusion and Future Work

In this thesis, RF energy harvesting from commercial Wi-Fi routers is studied. The goal is to design a novel system that is able to harvest and rectify Wi-Fi signals at low power levels. We conduct experiments in order to identify the challenges of efficient energy harvesting from ambient Wi-Fi signals. As a solution, we design, implement and evaluate a packet injection algorithm using the colasoft packet builder. The algorithm increases channel occupancy by injecting additional traffic in a controlled manner in order to avoid the intermittent reception of Wi-Fi signals. We measure the received power level from the Wi-Fi router with the proposed algorithm and compare it to a dedicated point-to-point transmission using a rectenna system. Moreover, we evaluate the effect of the packet injection algorithm on existing Wi-Fi users in the network using an experimental study with video streaming over smartphones. For this, we perform an analytical comparison and assess packet data captured using wireshark, in order to optimize the packet sizes and the inter-packet delay. As a result, we chose a packet size of 1000Bytes and an inter-packet delay of 1ms. The download duration of a 16.81MB video increased by 8.1% and the bit rate decreased by 5.1% due to the effect of the packet injection algorithm, which is regarded as an acceptable trade-off. To further explore performance under realistic operational conditions, we have also investigated the positive effect of interference from Wi-Fi routers in a given geographical area on the efficiency of energy harvesting, with focus on antenna gains, antenna patterns, routers spacing, and distance to the receiver. In the second complementary part of the thesis, we studied the performance of two different RF circuit designs as part of front-end power management units. These included proposed designs with passive and active components for RF wake-up and RF energy harvesting use cases. Detailed results are presented for both designs including a wide range of experiments in order to demonstrate performance effectiveness and identify existing trade-offs. Finally, we demonstrated the feasibility of utilizing the proposed packet injection algorithm and hardware designs in real systems using smart agriculture as a case study. This included two main studies: i. a study on using ambient Wi-Fi signals for wake-up and energy charg-

ing of sensors embedded in a field up to 50cm below ground level, with dry and wet sand; ii. as study on utilizing RF signals transmitted by drones for waking up sensors deployed in remote areas in a field.

As future work, we can further optimize the software based packet injection algorithm to be adaptive as a function of the Wi-Fi networks load in order to minimize impact on active users. Another research extension is to enhance the hardware RF circuit design by improving its energy efficiency while reducing the false wake-up, e.g., using some addressing mechanisms. In addition, massive antenna arrays can be used at the receiver side in order to improve the energy harvesting rate and extend the range between the transmitter and the receiver, which is important for large-scale areas.

Appendix A

Abbreviations

WSN	Wireless Sensor Networks
IoT	Internet of Things
M2M	Machine to Machine
M2P	Machine to Person
WEH	wireless Energy Harvesting
WuR	Wake-up Radio
MAC	Medium Access Protocols
WuRx	Wake-up Receiver
WuS	Wake-up Signal
FCS	Frame Check Sequence
DoS	Denial of Service
PSR	Packet Success Rate
CSMA/CA	Carrier Sense Multiple Access with Collision Avoidance
WUSN	Wireless Underground Sensor Networks
VWC	Volumetric Water Content
TDR	Time Domain Reflectometry

Bibliography

- [1] D. Evans, “The internet of things: How the next evolution of the internet is changing everything,” white paper, Cisco Internet Business Solutions Group, 2011.
- [2] R. Piyare, A. L. Murphy, C. Kiraly, P. Tosato, and D. Brunelli, “Ultra low power wake-up radios: A hardware and networking survey,” *IEEE Communications Surveys Tutorials*, vol. 19, pp. 2117–2157, Fourthquarter 2017.
- [3] D. Ng, E. Lo, and R. Schober, “Energy-efficient resource allocation in ofdma systems with hybrid energy harvesting base station,” *IEEE Transactions on Wireless Communications*, vol. 12, pp. 3412–3427, July 2013.
- [4] G. Tuna and V. Gungor, “Energy harvesting and battery technologies for powering wireless sensor networks,” in *Industrial Wireless Sensor Networks* (R. Budampati and S. Kolavennu, eds.), Woodhead Publishing Series in Electronic and Optical Materials, pp. 25 – 38, Woodhead Publishing”, 2016.
- [5] I. Krikidis, S. Timotheou, S. Nikolaou, G. Zheng, D. W. K. Ng, and R. Schober, “Simultaneous wireless information and power transfer in modern communication systems,” *IEEE Communications Magazine*, vol. 52, pp. 104–110, Nov 2014.
- [6] K. Huang and E. Larsson, “Simultaneous information and power transfer for broadband wireless systems,” *IEEE Transactions on Signal Processing*, vol. 61, pp. 5972–5986, Dec 2013.
- [7] Tmote Sky, *Ultra Low Power IEEE 802.15.4 Compliant Wireless Sensor Module, San Fransisco, CA, USA*, 2006.
- [8] P. P. Mercier and A. P. Chandrakasan in *Cham.Switzerland: Springer*.
- [9] D. Pozar, *Electromagnetic Theory. Microwave Engineering*, John Wiley and Sons, 4rth ed., 1998.

- [10] C. F. Liu, M. Maso, S. Lakshminarayana, C. H. Lee, and T. Q. S. Quek, “Simultaneous wireless information and power transfer under different csi acquisition schemes,” *IEEE Transactions on Wireless Communications*, vol. 14, pp. 1911–1926, April 2015.
- [11] S. Timotheou, I. Krikidis, S. Karachontzitis, and K. Berberidis, “Spatial domain simultaneous information and power transfer for mimo channels,” *IEEE Transactions on Wireless Communications*, vol. 14, pp. 4115–4128, Aug 2015.
- [12] A. A. Nasir, X. Zhou, S. Durrani, and R. A. Kennedy, “Relaying protocols for wireless energy harvesting and information processing,” *IEEE Transactions on Wireless Communications*, vol. 12, pp. 3622–3636, July 2013.
- [13] X. Chen, Z. Zhang, H. h. Chen, and H. Zhang, “Enhancing wireless information and power transfer by exploiting multi-antenna techniques,” *IEEE Communications Magazine*, vol. 53, pp. 133–141, April 2015.
- [14] D. Niyato, X. Lu, P. Wang, D. I. Kim, and Z. Han, “Distributed wireless energy scheduling for wireless powered sensor networks,” in *2016 IEEE International Conference on Communications (ICC)*, pp. 1–6, May 2016.
- [15] G. A. Vera, D. Allane, A. Georgiadis, A. Collado, Y. Duroc, and S. Tedjini, “Cooperative integration of harvesting rf sections for passive rfid communication,” *IEEE Transactions on Microwave Theory and Techniques*, vol. 63, pp. 4556–4566, Dec 2015.
- [16] M. Fantuzzi, D. Masotti, and A. Costanzo, “Simultaneous uhf energy harvesting and uwb-rfid communication,” in *2015 IEEE MTT-S International Microwave Symposium*, pp. 1–4, May 2015.
- [17] S. Kim, R. Vyas, J. Bito, K. Niotaki, A. Collado, A. Georgiadis, and M. M. Tentzeris, “Ambient rf energy-harvesting technologies for self-sustainable standalone wireless sensor platforms,” *Proceedings of the IEEE*, vol. 102, pp. 1649–1666, Nov 2014.
- [18] F. Goodarzy, E. Skafidas, and S. Gambini, “Feasibility of energy-autonomous wireless microsensors for biomedical applications: Powering and communication,” *IEEE Reviews in Biomedical Engineering*, vol. 8, pp. 17–29, Aug 2015.
- [19] C. Boyer and S. Roy, “Backscatter communication and rfid: Coding, energy, and mimo analysis,” *IEEE Transactions on Communications*, vol. 62, pp. 770–785, March 2014.

- [20] R. Correia, N. B. de Carvalho, G. Fukuday, A. Miyaji, and S. Kawasaki, "Backscatter wireless sensor network with wpt capabilities," in *2015 IEEE MTT-S International Microwave Symposium*, pp. 1–4, May 2015.
- [21] S. H. Choi and D. I. Kim, "Backscatter radio communication for wireless powered communication networks," in *2015 21st Asia-Pacific Conference on Communications (APCC)*, pp. 370–374, Oct 2015.
- [22] N. Jose, N. John, P. Jain, P. Raja, T. V. Prabhakar, and K. J. Vinoy, "Rf powered integrated system for iot applications," in *2015 IEEE 13th International New Circuits and Systems Conference (NEWCAS)*, pp. 1–4, June 2015.
- [23] M. M. Tentzeris, A. Georgiadis, and L. Roselli, "Energy harvesting and scavenging," *Proceedings of the IEEE*, vol. 102, pp. 1644–1648, Nov 2014.
- [24] X. Lu, P. Wang, D. Niyato, D. I. Kim, and Z. Han, "Wireless charging technologies: Fundamentals, standards, and network applications," *IEEE Communications Surveys Tutorials*, vol. 18, pp. 1413–1452, Secondquarter 2016.
- [25] L. Gu and J. A. Stankovic, "Radio-triggered wake-up for wireless sensor networks," in *Real Time System*, vol. 29, pp. 157–182, 2005.
- [26] SPICE, *SPICE SIMULATOR*. [Online]. Available: <https://www.seas.upenn.edu/jan/spice/PSpiceReferenceguideOrCAD.pdf>.
- [27] C. Chung, Y. H. Kim, T. H. Ki, K. Bae, and J. Kim, "Fully integrated ultra-low-power 900 mhz rf transceiver for batteryless wireless microsystems," in *2011 18th IEEE International Conference on Electronics, Circuits, and Systems*, pp. 196–199, Dec 2011.
- [28] P. Kamalinejad, K. Keikhosravy, M. Magno, S. Mirabbasi, V. C. M. Leung, and L. Benini, "A high-sensitivity fully passive wake-up radio front-end for wireless sensor nodes," in *2014 IEEE International Conference on Consumer Electronics (ICCE)*, pp. 209–210, Jan 2014.
- [29] D. D. Donno, L. Catarinucci, and L. Tarricone, "Ultralong-range rfid-based wake-up radios for wireless sensor networks," *IEEE Sensors Journal*, vol. 14, pp. 4016–4017, Nov 2014.
- [30] H. Sun, Y. x. Guo, M. He, and Z. Zhong, "A dual-band rectenna using broadband yagi antenna array for ambient rf power harvesting," *IEEE Antennas and Wireless Propagation Letters*, vol. 12, pp. 918–921, July 2013.

- [31] C. Song, Y. Huang, P. Carter, J. Zhou, S. Yuan, Q. Xu, and M. Kod, “A novel six-band dual cp rectenna using improved impedance matching technique for ambient rf energy harvesting,” *IEEE Transactions on Antennas and Propagation*, vol. 64, pp. 3160–3171, July 2016.
- [32] D. K. Ho, I. Kharrat, V. D. Ngo, T. P. Vuong, Q. C. Nguyen, and M. T. Le, “Dual-band Rectenna for Ambient RF Energy Harvesting at GSM 900 MHz and 1800 MHz,” in *2016 IEEE International Conference on Sustainable Energy Technologies (ICSET)*, pp. 306–310, Nov. 2016.
- [33] N. Tung, “Multi-band Ambient RF Energy Harvesting Rectifier for Autonomous Wireless Sensor Networks,” in *2016 IEEE Region 10 Conference (TENCON)*, pp. 3736–3739, Nov. 2016.
- [34] Y. Zhao, V. C. M. Leung, X. Sun, Z. Chen, and H. Ji, “Energy-Efficient Resource Allocation in Cellular Network with Ambient RF Energy Harvesting,” in *2017 IEEE Wireless Communications and Networking Conference (WCNC)*, pp. 1–6, Mar. 2017.
- [35] IEEE STANDARDS ASSOCIATION, 2017. [Online]. Available: http://www.ieee802.org/11/Reports/802.11_Timelines.htm.
- [36] Ericsson, *IOT Outlook*, June 2017. [Online]. Available: <https://www.ericsson.com/en/mobility-report/internet-of-things-outlook>.
- [37] J. F. Ensworth, S. J. Thomas, S. Y. Shin, and M. S. Reynolds, “Waveform-aware Ambient RF Energy Harvesting,” in *2014 IEEE International Conference on RFID (IEEE RFID)*, pp. 67–73, Apr. 2014.
- [38] G. A. Vera, A. Georgiadis, A. Collado, and S. Via, “Design of a 2.45 ghz rectenna for electromagnetic (em) energy scavenging,” in *2010 IEEE Radio and Wireless Symposium (RWS)*, pp. 61–64, Jan 2010.
- [39] V. Talla, B. Kellogg, B. Ransford, S. Naderiparizi, J. R. Smith, and S. Golakota, “Powering the Next Billion Devices with Wi-fi,” *Commun. ACM*, vol. 60, pp. 83–91, Feb. 2017.
- [40] U. Olgun, C. C. Chen, and J. L. Volakis, “Efficient ambient wifi energy harvesting technology and its applications,” in *Proceedings of the 2012 IEEE International Symposium on Antennas and Propagation*, pp. 1–2, July 2012.
- [41] U. Olgun, C. C. Chen, and J. L. Volakis, “Wireless power harvesting with planar rectennas for 2.45 ghz rfids,” in *2010 URSI International Symposium on Electromagnetic Theory*, pp. 329–331, Aug 2010.

- [42] J. F. Ensworth, S. J. Thomas, S. Y. Shin, and M. S. Reynolds, "Waveform-aware ambient rf energy harvesting," in *2014 IEEE International Conference on RFID (IEEE RFID)*, pp. 67–73, April 2014.
- [43] TP-Link, *TP-Link TL-WR541G 54 Mbps Extended Range Wireless Router*. [Online]. Available: <http://static.tp-link.com/resources/software/200977201065.pdf>.
- [44] DD-WRT, *DD-WRT: WAN OPTIMIZATION*. [Online]. Available: <http://www.dd-wrt.com/site/index>.
- [45] Colasoft, *Colasoft Packet Builder*, 2016. [Online]. Available: http://www.colasoft.com/packet_builder/.
- [46] Firewall, *The Ethernet II Frame Format*, 2013. [Online]. Available: <http://www.firewall.cx/networking-topics/ethernet/ethernet-frame-formats/201-ethernet-ii.html>.
- [47] C. H. P. Lorenz, S. Hemour, and K. Wu, "Physical Mechanism and Theoretical Foundation of Ambient RF Power Harvesting Using Zero-Bias Diodes," *IEEE Transactions on Microwave Theory and Techniques*, vol. 64, pp. 2146–2158, July 2016.
- [48] C. R. Valenta, "Fundamental Limitations for Schottky Diode RF Energy Harvesting," in *2015 IEEE International Conference on RFID Technology and Applications (RFID-TA)*, pp. 188–193, Sept. 2015.
- [49] Linear Technology, *Nanopower Comparator with Reference*, 2007. [Online] <https://www.analog.com/media/en/technical-documentation/data-sheets/1540fb.pdf>.
- [50] H. Khodr, N. Kouzayha, M. Abdallah, J. Costantine, and Z. Dawy, "Energy efficient iot sensor with rf wake-up and addressing capability," *IEEE Sensors Letters*, vol. 1, pp. 1–4, Dec 2017.
- [51] Texas Instrument, *CC3200 SimpleLink Wi-Fi*, Feb 2015. [Online]. Available: <http://www.ti.com/lit/ds/symlink/cc3200.pdf>.
- [52] Texas Instruments, *LMC6001 Ultra, Ultra-Low Input Current Amplifier*. [Online]. Available: <http://www.ti.com/lit/ds/symlink/lmc6001.pdf>.
- [53] Linear Technology, *Ultralow Voltage Step-Up Converter and Power Manager*. [Online]. Available: <http://www.analog.com/media/en/technical-documentation/data-sheets/3108fc.pdf>.
- [54] Würth Elektronik, *1:20 Transformer*. [Online]. Available: <https://katalog.we-online.com/pbs/datasheet/74488540250.pdf>.

- [55] C. Balanis, "John wiley and sons," in *Modern Antenna Handbook*, 2007.
- [56] Panasonic, *Charge Methods For NiCd Batteries*, August 2003. [Online]. Available: <http://www.rathboneenergy.com/articles/PanasonicNiCdChargeMethods.pdf>.
- [57] D-Robotics, *DHT11 Humidity & Temperature Sensor*, Jul 2010. [Online]. Available: <http://www.micropik.com/PDF/dht11.pdf>.
- [58] M. C. Vuran and A. R. Silva, "Communication through soil in wireless underground sensor networks theory and practice," in *Sensor Networks, Signals and Communication Technology* (G. Ferrari, ed.), Springer-Verlag Berlin Heidelberg, 2010.
- [59] I. Akyildiz and E. Stuntebeck, "Wireless underground sensor networks: research challenges," *Ad Hoc Networks Journal* 4, pp. 669–686, 2006.
- [60] I. Akyildiz, Z. Sun, and M. Vuran, "Signal propagation techniques for wireless underground communication networks," *Physical Communication Journal* 2 (3), pp. 167–173, 2009.
- [61] L.Li, M.Vuran, and I.Akyildiz, "Estimation of soil-water characteristic curves in multiple-cycles using membrane and tdr system," *Med-Hoc-Net*, 2016.
- [62] I. Akyildiz and M. Vurana, "Channel model and analysis for wireless underground sensor networks in soil medium," 2010.
- [63] W. Hong, Y. Jung, S. Kang, and J. Lee, "Characteristics of underground channel for wireless underground sensor networks," *Environmental and Architectural Engineering, Korea University*, 2007.
- [64] E. P. Stuntebeck, D. Pompili, and T. Melodia, "Wireless underground sensor networks using commodity terrestrial motes," in *2006 2nd IEEE Workshop on Wireless Mesh Networks*, pp. 112–114, Sept 2006.